inorganics

MDPI

Review

MOFs for Electrochemical Energy Conversion and Storage

Claudio Pettinari [1,2,*] and Alessia Tombesi [1]

[1] Chemistry Section, School of Pharmacy, University of Camerino, Via S. Agostino 1, 62032 Camerino, Italy
[2] Istituto di Chimica dei Composti Organometallici (ICCOM-CNR), Via Madonna del Piano 10, 50019 Sesto Fiorentino, Italy
* Correspondence: claudio.pettinari@unicam.it

Abstract: Metal organic frameworks (MOFs) are a family of crystalline porous materials which attracts much attention for their possible application in energy electrochemical conversion and storage devices due to their ordered structures characterized by large surface areas and the presence in selected cases of a redox-active porous skeleton. Their synthetic versatility and relevant host-guest chemistry make them suitable platform for use in stable and flexible conductive materials. In this review we summarize the most recent results obtained in this field, by analyzing the use of MOFs in fuel and solar cells with special emphasis on PEMFCs and PSCs, their application in supercapacitors and the employment in batteries by differentiating Li-, Na- and other metal ion-batteries. Finally, an overview of the water splitting reaction MOF-catalyzed is also reported.

Keywords: MOFs; polymers; fuel cells; solar cells; batteries; water-splitting reaction; supercapacitors; composites

Citation: Pettinari, C.; Tombesi, A. MOFs for Electrochemical Energy Conversion and Storage. *Inorganics* **2023**, *11*, 65. https://doi.org/10.3390/inorganics11020065

Academic Editor: Francis Verpoort

Received: 17 December 2022
Revised: 22 January 2023
Accepted: 27 January 2023
Published: 30 January 2023

1. Introduction

The world needs more power, preferably in a clean and renewable form. This request is the main driver for new materials development. It is now pressing that energy-harvesting materials are produced, suitable to maximize the efficiency of electrochemical energy conversion and storage devices, such as fuel cells, solar cells, supercapacitors, and batteries, which are fundamental technologies for green energy sources and can be used to replace fossil energy. Metal organic frameworks (MOFs) are a potentially attractive and valid alternative to several materials to date employed in most of the devices above. They are highly porous compounds with tunable compositions specially adapted for applications in diverse areas such as drug delivery [1], gas adsorption [2], separation [3], energy storage and conversion [4]. They are constructed from the self-assembly of metal ions or clusters and organic ligands that generates topologically diverse and well-defined structures via coordination bonds [5]. More recently, research on MOF-based materials for electrochemical energy storage and conversion has attracted tremendous interest in next-generation rechargeable battery applications [6]. The easy tuning of the metal and organic constituent components in MOFs allows the incorporation of electroactive sites, typically redox-active metal centers (Fe, Co, Ni, Mn, etc.) [7]. In addition, the porous structure of MOFs enables facile electrolyte penetration and ion transportation [8]. However, an appreciable number of MOFs suffers from insufficient electronic conductivity and from the low tap density and structural degradation during the recharge process, which could limit their practical application [9]. To overcome these limitations, MOF-based composite materials [10], obtained by combining MOFs with conductive materials (e.g., carbon, polymers, metals) [11] and MOF-derived materials possessing nanostructures typical of metals/oxides/hydroxides or nanoporous carbons originated from controlled conversion conditions (e.g., atmosphere and temperature) are very promising electrode materials [10].

There are many excellent reviews on MOFs and their derivatives employed in energy conversion and storage systems (ECS) [9,12–31]. For this reason, we mainly restrict our

focus to studies reported in 2022, highlighting recent progress in the use of pristine MOFs, MOF composites and other MOF derivatives for next-generation rechargeable batteries, solar cells, fuel cells and supercapacitors. We discuss here the design and synthesis of various MOFs and MOF-related materials and their components, their structures, and the advantageous properties to enhancing performances in energy conversion and storage devices.

2. Fuel Cells

A fuel cell is a device able to generate electricity, heating and cooling from clean natural gas or renewable biogas through an electrochemical reaction. Fuel cell energy provides a reliable supply of ultra clean energy, and for this reason this device is already used in a broad range of applications as power source.

In the electrochemical cells, the chemical energy of a fuel (often hydrogen) and of an oxidizing agent (often oxygen) is directly converted into electrical energy through a pair of redox reactions. Each individual cell contains an anode, a cathode, an electrolyte membrane and an external circuit [31].

A typical fuel cell works by oxidizing hydrogen to protons at the anode site. The protons migrate through the electrolyte to the cathode, where oxygen molecules are reduced to oxide ions and then H^+ and O^{2-} reacts to form water. The electrons go through an external circuit, generating a flow of electricity and heat.

Depending on the nature of the electrolyte employed, fuel cells can be classified according to the type of the electrochemical reaction which takes place in the cell. This classification determines also the temperature at which the cell operates, the required catalyst and fuel and other factors affecting the ultimate application of the cells [32].

In a proton exchange membrane- or polymer electrolyte membrane-fuel cell the electrolyte is a solid polymer membrane in which protons are mobile and platinum is the catalyst. Its operative temperature is below 100 °C but pure hydrogen must be used. When the hydrogen is supplied by liquid methanol, the cells are called direct methanol fuel cells [33,34]. A high temperature PEMFC (HT-PEMFC) operates up to 200 °C by using a mineral acid-based system in the cell [35]. Even in the "alkaline fuel cell" (AFC) and "phosphoric-acid fuel cell" (PAFC), pure hydrogen is required to be supplied to the anode. In the "solid oxide fuel cell" (SOFC) and "molten carbonate fuel cell" (MCFC), where a solid ceramic electrolyte and molten carbonate salt suspended in a porous ceramic matrix are used as electrolyte, respectively, CO, H_2, and other organic intermediates can be electrochemically oxidized at the anode. High-temperature operations are required but the fuel-processing reaction can be completed within the stack providing high electric efficiency [36–39].

2.1. PEMFC

PEMFC-type (Figure 1) are the most common employed fuel cells both in research and in commercial use, but they currently have a few limitations. Expensive noble metal-based catalysts, as for example platinum and platinum alloys, are necessary to accelerate the slow reactions at the anode and cathode. In addition, the polymer electrolyte membrane should be a good proton conductor and electron-insulating, to allow protons to flow from the anode to the cathode while forcing the electrons to travel through the external circuit [40].

In this scenario, MOFs have been surprisingly considered good candidates for enhancing proton conduction performance compared to other conventional materials [41,42]. MOFs in fuel cells can be used both in membrane and catalysts, with the requirement for this application being different.

An interesting example of synthesis of a Fe, N co-doped carbon catalyst for the ORR has been recently reported: the method involves the carbonization of a core-shell composite precursors where the shell is a Fe(III) porphyrin based conjugated polymer and the core is an N-doped porous carbon obtained from ZIF-8 (Figure 2). This material exhibits easily accessible single metal sites which efficiently catalyze electrochemical reactions in fuel-cells [43].

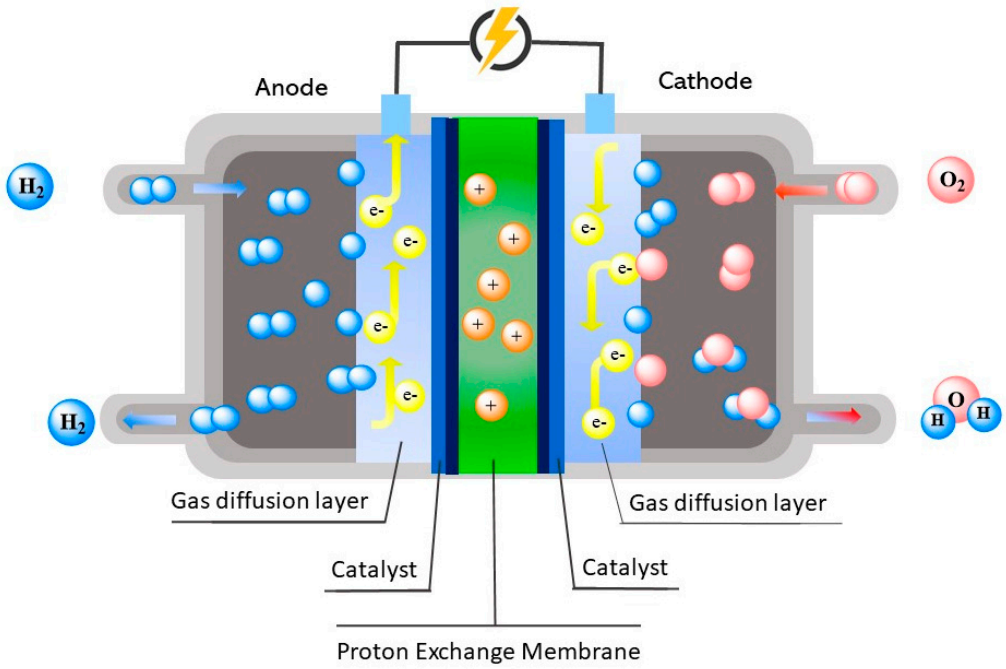

Figure 1. General scheme of a PEMFC.

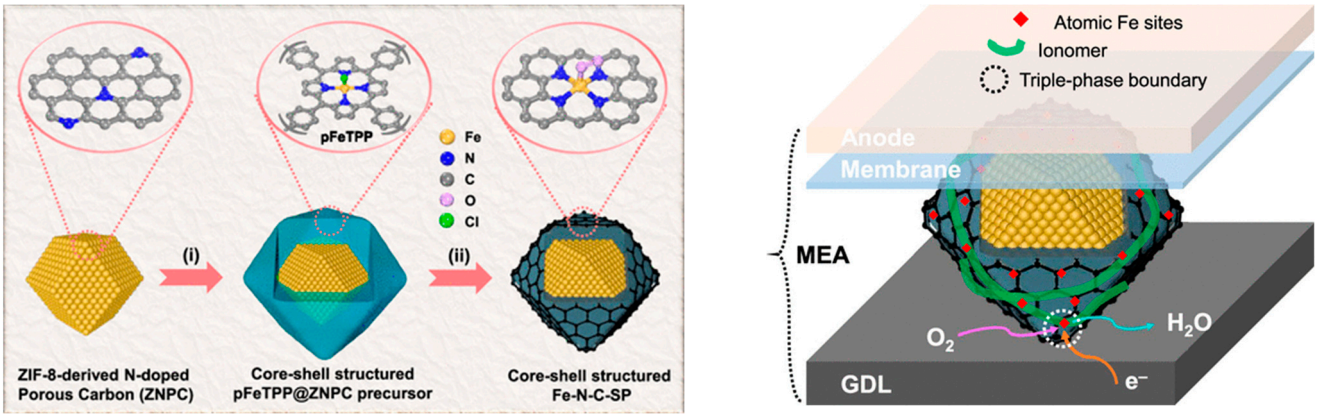

(**a**) (**b**)

Figure 2. (**a**) The synthesis of the core-shell Fe-N-C catalyst. (**b**) The membrane electrode assembly (MEA). Adapted from Ref. [43].

To improve the proton conductivity under variable humidity of Nafion, which is a standard solid electrolyte for most energy conversion and storage equipment, 3D core shell ZIF-8@PCM composites have been synthesized via an in situ growth method employing PCMs. Nafion/ZIF-8@PCMs with 1% of ZIF-8@PCMs content, exhibited high proton conductivity, 0.24 S cm^{-1} at 80 °C and 100% RH, 1.5 times higher than the recast Nafion membrane. This performance can be ascribed to a better dispersion of the ZIF-8@PCMs spherical structure in the Nafion matrix. The 2-methylimidazole ligand in ZIF-8, acting as both H-donor and acceptor, facilitates protons conduction. Moreover, the N–H group in the 2-methylimidazole interacts with the $–SO_3H$ group in Nafion, resulting in acid-base pairs at the interface which reduce the energy barrier for protons transport [44].

The presence of defects within the MOF crystal lattice can significantly affect the physical properties [45]. In the hybrid UiO-66/Nafion composite systematic defects in UiO-66 improve the overall proton conduction. Classical molecular-level structural and dynamics simulation in hybrid UiO-66/Nafion showed water molecules diffusing more

rapidly in the UiO-66-2wt%-pristine/defect where structure is more phase-segregated. In the low-concentration doped system, water molecules are bonded to accessible Lewis acid sites in defected Zr-nodes and the steric hindrance of UiO-66 compacts the polymers chains, changing the hydrophilic/water domains in hybrid membranes [46].

An increased metal cluster connectivity in Zr(IV)-based MOFs is able to improve effectively proton conductivity. $[Zr_6O_4(OH)_8(H_2O)_4(BPDC(SO_3H)_2)_4]$ (BUT-76) and $[Zr_6O_4(OH)_4(BPDC(SO_3H)_2)_6]$ (BUT-77) were synthesized by reaction of (2,2′-disulfo-[1,1′-biphenyl]-4,4′-dicarboxylate) with different quantity of connected Zr_6 cluster. BUT-77, with an *fcu* net connecting 12 $Zr_6O_4(OH)_4$ cluster exhibits denser hydrogen-bond interactions with water molecules creating more pathways for the proton migration [47]. BUT-77 demonstrated high proton conductivity at 80 °C and 100% relative humidity (RH) (the values range from $8.55 \cdot 10^{-3}$ for BUT-76 to $3.08 \cdot 10^{-2}$ S cm^{-1} for BUT-77) and proton conductivity of 1.25 10^{-3} S cm^{-1} at 80 °C, 100% RH for BUT-77 mixed-matrix membrane.

ZIF-8(Fe) has been used as precursor for the synthesis of an ORR catalyst with ultrathin sheet g-C_3N_4 (CN-UC) ultrasonically crushed. The carbonated-ZIF(Fe)/CN-UC catalyst showed a porous and uniform structure with several Fe-N_x active sites maintaining the original zeolite-type structure of ZIF-8. The etching agent CN-UC improves the stability of the etched catalyst. The durability of ZIF(Fe)/CN-UC in PEMFCs was higher than that of commercial Pt/C (the performance only decreases by 11% after 100,000 S durability test), but the measured ORR performance is slightly lower. The maximum power densities of ZIF(Fe)/CN-UC catalysts reached 0.484 W·cm^{-2} [48].

Zn_4O(1,4-benzenedicarboxylate)$_3$ (MOF-5) has been used as efficient precursor to prepare porous carbon support (C-MOF-5) to produce Fe SACs. The hierarchical porosity of C-MOF-5 offers a high specific area to accommodate large amount of Fe-N_x active sites (2.35%). These highly dispersed and fully exposed to O_2 Fe-N_x sites increased the ORR activity of Fe SAC-MOF-5 with an $E_{1/2}$ of 0.83 V (vs RHE) in 0.5 m H_2SO_4. The 0.2 MPa H_2-O_2 PEMFC assembled with Fe SAC-MOF-5 as the cathode catalyst achieves a peak power density of 0.83 W cm^{-2} [49].

2.2. DMFC

MOFs can play an important role in designing efficient DMFCs, as they can be functionalized with multivalent ligands and metal centers improving fuel cells power. It has been reported the presence of O atoms in the MOFs improves the poison resistance of the composites, whereas composites based on graphene and MOFs are very interesting for the conductivity and low cost. Nanomaterials coupled to MOFs exhibit improved electron transfer properties [50]. Some details concerning the most important steps toward commercialization also for MOFs-based DMFC are recently reviewed [51]. It is now well known that the presence of amino-sulfonic acid-based bi-functionalized MOFs as inorganic nanofillers increase the performance of PAEK (poly(arylene ether ketone)) hybrid membranes in DMFCs. The synthesis of an MOF useful to facilitate the formation of proton transfer channels is reported in Figure 3 [52].

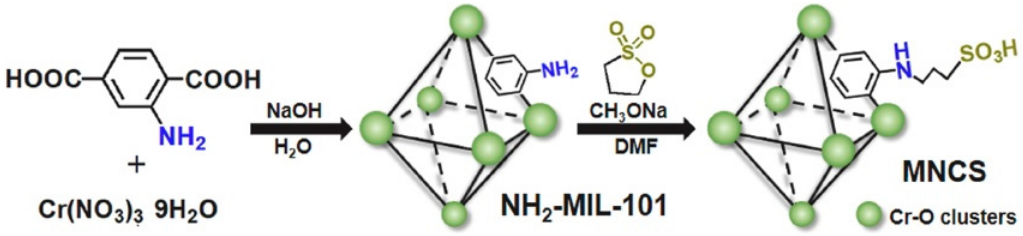

Figure 3. The synthesis of an amino-sulfonic acid-based bi-functionalized MOF (adapted from Ref. [52]).

A graphene-based FeO/NiO MOF composite prepared by using terephthalic linkers has been demonstrated to be a valid catalytic material for methanol oxidation in DMFC [53].

3. Solar Cells

3.1. PSCs

Today, MOFs are important candidates to improve the performance of PSCs (which are promising components of photovoltaic devices), especially if they suffer of a great instability due to degradation induced by several factors such as moisture, UV and temperature.

The development of MOF-assisted perovskite photovoltaic devices has been clearly reviewed, all possible functions for MOFs being analyzed, i.e., the role of individual layer, or of modifier of the interlayer and finally that of MOF/perovskite heterojunction [54]. Particular emphasis has been given to the possibility to tune the MOFs' bandgap and the semiconducting properties by careful choice of the electron-rich metal nodes and of the organic molecules, as also the pore and particle sizes which can affect the quality of the perovskite film formation. PSCs are formed by a light absorption layer, a hole transport layer and an electron transport layer. Several researchers reported important modifications as the replacement of organic with inorganic cations and the use of perovskite passivation techniques: moisture-stable PSCs can be produced by hybridization of a hygroscopic copper(II) benzene carboxylate MOF with a light-absorbing perovskite layer, the MOF being able to attract the moisture [55]. The perovskite-MOF hybrid in Figure 4 shows high stability in air under dark conditions up to 22 months, whereas the analogous perovskite layer without MOF rapidly decomposes into PbI_2. The system perovskite-MOF also improves the transfer of photo-excited electrons from the perovskite to TiO_2, the MOF making available additional channels for electron extraction.

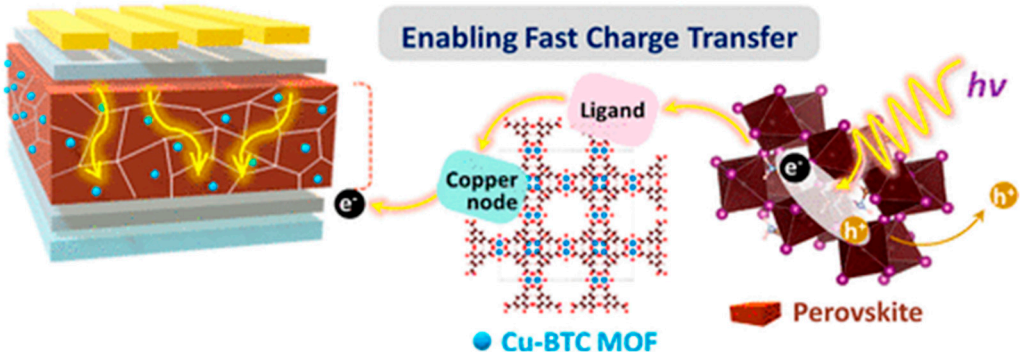

Figure 4. The light-absorbing hybrid layer in a PSC. Adapted from Ref. [55].

Polynuclear rare-earth MOFs based on Tb and tetrazole-benzoate ligands are also ideal additives for the hole transport layer to improve the efficiency of PSCs. The presence of both N and O atoms in the MOFs is fundamental as they can interact with the uncoordinated Pb and passivate the surface defects of the perovskite film. These MOFs are very stable to moisture and temperature exposure and are very good candidates for hole transport layer to prevent H_2O attack to PSCs [56].

Na-doped TiO_2 obtained by the precursor MIL-125(Ti) has been inserted into the interlayer between the electron transport and perovskite layer. In this manner the interface contact between the two layers results improved, and an enhancement of the optoelectronic performance of the PSCs has been observed [57].

The interaction of a perovskite precursor grown along the skeleton of an MOF based on Zn and polydentate ligand built with heterocyclic triazole and tetrazole rings yielded a macromolecular intermediate phase and subsequently a perovskite film with enhanced stability. This strategy allowed improvement in the volatility and directed the self-organization of small molecules used as additives in PSCs. After MOF doping, the degradation activation energy of PSCs increases by up to 174.01 kJ mol^{-1} [58].

The PSCs suffer not only for the short-term stability but also for the toxicity due to leaked lead ions. A chemical doping strategy based on the use of POMs-MOFs (P@Ms) host-guest nanostructured dopants produces a functionalized P@Ms able to restrict the

migration and leakage of the Pb^{2+} ions from the degraded PSCs due to the presence of the active sites in a P@Ms prepared from $H_3PMo_{12}O_{40}$ and zirconium-porphyrin MOF [59].

3.2. Other Solar Cells

MOFs can be also employed in DSSC fabrication. For example, a MIL-101-doped TiO_2 film obtained by a sol-gel method deposited on a fluorine-doped tin oxide layer enhances the efficiency of DSSC, as confirmed by spectral data. The power conversion efficiency of a hybrid containing MIL-101 and TiO_2 is 8.687% under 100 mW/cm^2 illumination power and 1.85 times greater than that measured for undoped DSSC. The energy band alignment, the strong increase in dye adsorption and finally the grow of photoelectron trapping are all factors determining the enhancement of the efficiency [60].

A $Cu^{+1/+2}$ redox mediator containing pyridine and bipyridine ligands, together with a Co-MOF and an aqueous geltrite polymer, demonstrated very good performance in DSSC. The higher J_{sc} and PCE is supported from the high conductivity, larger charge and higher chemical capacitance [61].

A bimetallic MOF based on Cu and Ni loaded on indium tin oxides has been investigated as anode in microalgae based biophotovoltaic cells. Its influence in green energy production is by using the freshwater microalgae *Chlorella* sp. UMACC 313 as a catalyst has been investigated. This system demonstrated elevated structural integrity and significant electrochemical activeness [62].

Cu_2S-containing chalcogenide solar cells are very important materials for photovoltaic industry; however, several problems often prevent their use as, for example, the degradation or the copper ion diffusion. A bipyridine-containing Cu-MOF has been used as copper source as the Lewis basic bipyridine site is able to store Cu(I) ion and compensates, when required, the diffused copper ions. The use of a Cu(I)-MOF can enhance the stability of $Cu_{2-x}S$/CdS photovoltaic cells [63].

MOFs can be also employed in PECs that directly convert absorbed photons into chemical fuels, as they can be incorporated into PECs by installing molecular light harvester and molecular catalysts within the pores [64].

4. Batteries

From mobile devices to electric vehicles, all are dependent on portable sources of energy: batteries. Batteries consist of a series of connected electrochemical cells which store chemical energy and convert it to electrical energy through electrochemical reactions involving the flow of electrons from one electrode to another across an external circuit, generating an electric current [65]. The two electrodes, anode and cathode, are separated by a solid, liquid or viscous electrolyte in which charged ions balance the electrons flow [66,67]. During the discharging process, the anode provides electrons to the external circuit through the oxidation reaction, and the electrons are collected at the cathodes through the reduction reaction. The reverse reaction takes place when the charging process is running, and the battery is recharged by applying an external voltage to the two electrodes. The nature of the electrodes and electrolytes determines the chemical reactions affecting the battery, the stored energy, and its voltage. Considerable efforts have been devoted to the exploration of effective electrode materials capable of delivering high electrochemical performance.

Metal-ion batteries are a class of rechargeable batteries in which the metal ions provide energy by flowing from the negative electrode to the positive electrode. During the charging process, metal ions are deintercalated from the cathode and then migrate through the electrolyte and intercalate to the anode storing energy. When the battery is discharging, metal ions move back to the cathode realizing energy [25]. Lithium-ion batteries (LIBs) are the most common rechargeable battery employed as energy storage devices in consumer electronics and electric vehicles. The limited energy density and the high cost of LIBs have been the driving force behind the exploration and development of new electrode materials, such as sodium-ion batteries (SIBs), which have larger theoretical capacities per ion and

more abundant metal-ion precursors. However, low specific capacity and limited rate performance are the current challenges in metal-ion batteries [68].

Several studies have been focused on cathode and anode materials to overcome conventional electrode materials with limited energy/power density and short cycle life. A recent review reported a summary of electrochemical properties of MOFs recently employed in battery cathodes, dedicating special attention to MOF-derived nanocomposites [69] whereas an article published in 2021 described the use of pristine MOFs and MOFs-derived materials as an anode in lithium-ion batteries [70].

High surface area and tunable pores in MOFs can provide channels for ion-transportation within the electrode, enhancing the performance of the energy storage devices [32,71]. The porous structures offer opportunities to incorporate electroactive sites making MOFs excellent candidate as advanced electrode materials for battery systems [30]. Poor electrical conductivity, low tap density and structural degradation after the recharge process of MOFs are still relevant issues in the MOF-based electrodes that may be detrimental to their practical use. However, to overcome these problems, MOF-composite materials can be obtained combining MOFs with conductive materials such as carbon, polymers, and metals. Moreover, MOFs are ideals precursors to design MOF-derived materials with nanostructures typical of metals/oxides/hydroxides or nanoporous carbons by strict control of the conversion conditions (e.g., atmosphere and temperature) [72,73].

4.1. Li-ion Batteries (LIBs)

Lithium-ion batteries have received significant attention in the commercial battery market, owing to their high cell voltage, low self-discharge rate and long cycle stability. However, low energy density (100–220 $Wh \cdot kg^{-1}$) and high cost are the main limitations in the practical applications of such batteries. At present, most LIBs utilize a graphite-based anode material and a metal oxide cathode, have low theoretical capacity of ~350 mAh g^{-1} and limited rate capability [68]. Moreover, an irregular transport of ions during cycling causes Li dendrites formation, leading low coulombic efficiency. Thus, porous carbons, alloys, transition metal oxides and silicon materials have been studied as alternative electrode materials with a promising high specific capacity and charge/discharge rate, but they still suffer of huge volume change and their capacity quickly fades upon cycling [74].

The porous and stable structure of MOFs can facilitate lithium intercalation/deintercalation promoting the Li^+ diffusion, preventing structural degradation and reducing side reactions. The control of metal centers and organic ligands can provide a large number and high density of redox-active sites to increase battery capacity. Moreover, the morphologies of MOF-composites generate unique nanostructures offering remarkable cycle life and excellent rapid charge-discharge capability [74].

Melt-quenched MOF glasses are a new family of glass materials in which the crystalline structure of amorphized MOFs showed a thermal conductivity higher than their crystalline counterparts owing to a high degree of short-range disorder [75,76]. The melt-quenched ZIF-62(Co) ($Co(Im)_{1.75}(bIm)_{0.25}$) glass (ImH = imidazole) has been used to develop an anode for LIBs with carbon black and binder. It was found that this anode exhibits not only high specific capacity (306 mA h g^{-1} after 1000 cycles at the current density of 2 A g^{-1}) but also cycle stability, rate capability and larger capacity compared with the crystalline ZIF-62(Co) and the amorphous one prepared by high-energy ball-milling. This study highlights that the increased distortion and local breakage of the Co-N coordination bonds into the ZIF-62 network due to the insertion and extraction of Li^+ ions, creates additional channels for Li^+ ion diffusion and storage [77].

An ultramicropore Tostadas-shaped structure has been fabricated starting from one-pot hydrothermal synthesis of $(Ni_3(HITP)_2$ (HITP = 2,3,6,7,10,11-hexaiminotriphenylene) nanosheets (NHS) and Ni-HITP particles (NHP). Both NHS and NHP have been then mechanically electrostatic assembled into Tostadas-shaped (NHM) structure by controlled ball milling treatment. The Tostadas-architecture improves the adsorption capacity for Li^+ and its stability. The electrochemical performance of obtained NHM anodes gave a

superior reversible capacity of 1280 mA h g^{-1} cycles after 100 cycles at the rate of 0.1 A g^{-1} and its capacity was maintained at 392 mA h g^{-1} at 1 A g^{-1} after 1000 cycles [78].

The crystalline porosity of MOFs provides efficient and reversible ionic insertion/extraction, whereas the open metal cations provide active sites for effective redox reactions. Higher electrochemical performance can be gained by redox active metal sites and organic linkers. Ferrocenedicarboxylate has been employed as an efficient stable cathode for LIB, its unique structure and low solubility as well as the reversible redox shuttle of Fe^{2+}/Fe^{3+} being the cause of a high energy density of 549 Wh kg^{-1} (vs. lithium anode) and superior electrochemical performance [79].

A one-dimensional π-d conjugated coordination polymer based on high performance sodium-ion batteries has been prepared. The electrochemical process undergoes a three-electron reaction, the structure changing from C=N double bonds and Ni(II) to C−N single bonds and Ni(I), respectively [80].

Conjugated CPs are an important family of compounds employable as redox-active materials. Nanostructured d-p conjugated Ni species based on diamino- and dithiolene-derived ligands showed a high reversible capacity of 1164 mAh g^{-1} up to 1500 cycles and a fully rechargeable ability in 67 s and exhibit potential as coordination-polymer based electrodes (Figure 5) [81].

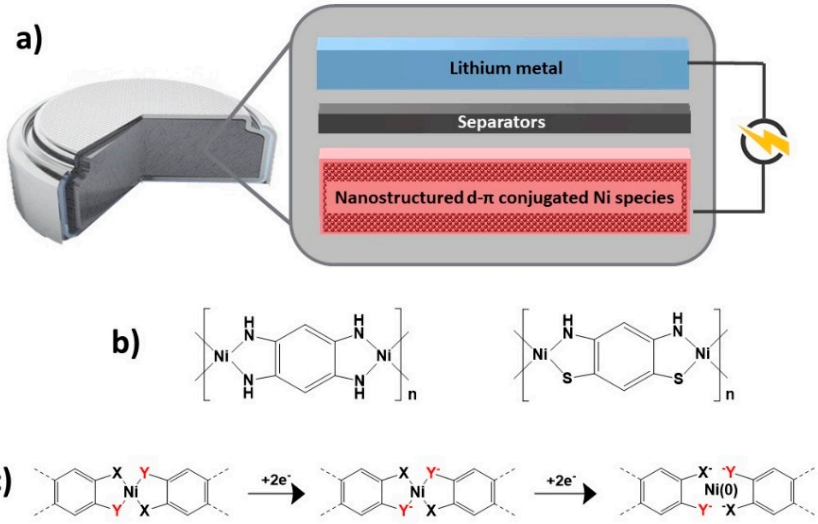

Figure 5. (**a**) A scheme of a hybrid electrochemical cell based on nanostructured d-p conjugated CPs. (**b**) Chemical structures of Ni-NH and Ni-S compounds. (**c**) Schematic mechanism of d-π conjugated coordination compounds on the basis of metal and organic ligand redox reactions (Ref. [81]).

In the iron (III)-tetrathiolate-terephthalate (Fe-TTTP) MOF based on multi-thiol dicarboxylate linker, the redox active Fe(III) ion in synergy with the π-conjugated multi-thiol motif is able to delocalize electrons enhancing stability and conductivity. The Fe-TTTP anode showed high cycling stability (310 ± 20 mAh g^{-1} at 2000 mA g^{-1} for 5000 cycles) with reversible capacity of 950 mAh g^{-1} at 50 mA g^{-1} and excellent rate performance (95 mAh g^{-1} up to 10,000 mA g^{-1}, 1.1 min for one cycle) [82].

A rod-shaped trimetallic MOF, NiFeMn(benzene-1,2,4,5-tetracarboxylate), showed, as anode, high specific capacity, and cycle stability (624 mAh g^{-1} at 100 mA g^{-1} over 100 cycles). The synergistic effect of multi-metal mixing sites and the strong π-π interactions of the conjugates carboxylate linker enhance rate performance owing to the high number of sites for intercalation-extraction of Li^+ [83]. Also, in a microsphere of the manganese and cobalt trimesic dual-MOF $Mn_2Co(C_9O_6H_3)_2$, the presence of two metal ions and the intercalation/deintercalation mechanism due to the carboxyl groups and benzene rings of the trimeric acid ligand, enhanced Li storage capacity (337 mAh g^{-1} after 600 galvanostatic charging/discharging cycles at 1000 mA g^{-1}). High capacity and good rate performance

have been recorded (819 mAh g^{-1} at 200 mA g^{-1} after 200 cycles and 148 mAh g^{-1} at 4000 mA g^{-1} respectively) [84].

The delocalization of electrons within an MOF can be promoted by introducing multiple metal ions in the frameworks. An MOF (FLaN) incorporating Fe^{2+}, Ln^{3+} and Na^{+} (Ln = La, Ce and Pr) has been fabricated by iono-thermal method. Its asymmetric unit and the different coordination environments of metal ions in the 3D structures guarantee straight passage for electrons during the recharge process of Li^{+} ion. The FLaN-MOF maintained a good cycle stability (349 mAh g^{-1} and 204 mAh g^{-1} after 300 cycles) [85].

A 2D HAGO layer demonstrated to be a promising material in electrochemical energy storage owing to fast carrier mobility and large electronic conductivity. Although its high electrochemical activity and strong structural stability, the large void spaces between the vertically aligned 2D nanosheets in the electrode structure reduce the volume density of the electrode [86–88]. To increase the low specific capacity (<200 mA h g^{-1}) and solve the problem of the limited ions transport, a ZIF-67-derived Co@CN was grown on HAGO by a freeze-casting method [89]. The HAGO/Co@CN electrode demonstrated a stable cycling at high areal capacity of 5.2 mA h cm^{-2} and high mass loading besides a capacity retention of >95% over 50 cycles. The introduction of Co@CN increases the electron/ion transport ability of the layered HAGO/Co@CN electrode as well as favorable lithium storage kinetics [90].

The MOF MIL-125(Ti) has been synthesized via solvothermal method using Pluronic F127 as structure-directing agent with the aim to obtain truncated octahedron gem shape. Then, after its thermal treatment an MOF-derived TiO_2 was obtained. Then, on the 3D mesoporous TiO_2, MoS_2 nanosheets were grown. The electrode made from this truncated TiO_2@C@MoS_2 hierarchical composite provided abundant active interfacial sites for lithium storage and the vertical structure facilitated the penetration of electrolyte. Large capacity at a various rate (~1075 mAh/g at 0.5 C and ~918 mAh/g at 2 C) and excellent cycle stability at a high rate (~958 mAh/g at 0.2 C) were observed [91]. A Bi-based MOF (CAU-17) has been used as precursor to fabricate MOF-derived Bi_2S_3 hybrid nanofibers coated by organic framework via polymerization and sulfidation processes. The obtained coating tolerates the volume expansion and active sulfide loss, improving reversible capacity, durability, and rate capability of metal sulfide [92].

A ZnNC electrode has been obtained after ZIF-8 annealing under N_2. The microporous ZIF-8 has been transformed in a mesoporous Zn–N-doped carbon material with a decreased surface area and an increased pore size which enhances the electronic conductivity. High-capacity retention rate was revealed by the higher discharge and charge capacities of 826 and 447 mA h g^{-1}, respectively [93].

An MOF-composite based on coated porous Co-Zn oxide and highly conductive 2D layered metal carbides MX-ene (Ti_3C_2) can be easily prepared. After the annealing process the porous ZnO/Co_3O_4 polyhedron obtained has been introduced into layered Ti_3C_2 nanosheets through electrostatic interaction due to the presence of an abundant surface functional group T_x (-F, –OH) in the MXene nanosheets. The performance of the LIBs assembled with hierarchical Ti_3C_2@Co_3O_4/ZnO composite as anode and AC as cathode showed an ultra-high energy density of 196.8 Wh/kg at a power density of 175 W/kg. These high electronic performances are ascribed to the presence of abundant active sites and open channels to accelerate Li^{+} transport in porous ZnO/Co_3O_4, the conductive Ti_3C_2 providing a faster ion and electron transfer [94].

An MOF based on Sn and 1,2-benzene-dicarboxylate was obtained by low-temperature aqueous solution method and used as anode material directly in LIBs without high temperature treatment. The stable layered network structure achieves a high reversible capacity of 1530 mAh g^{-1} after 400 cycles at a current density of 0.5 A g^{-1}, and long-cycle stability [95]. The excellent electrochemical performance is due the efficient electron transport channels in which Sn and O atoms can provide multiple active sites for lithium storage (Figure 6). Two reversible chemical reactions occur in the sites: the super lithiation of organic molecules and the alloying reaction of Sn atoms with lithium ion [96].

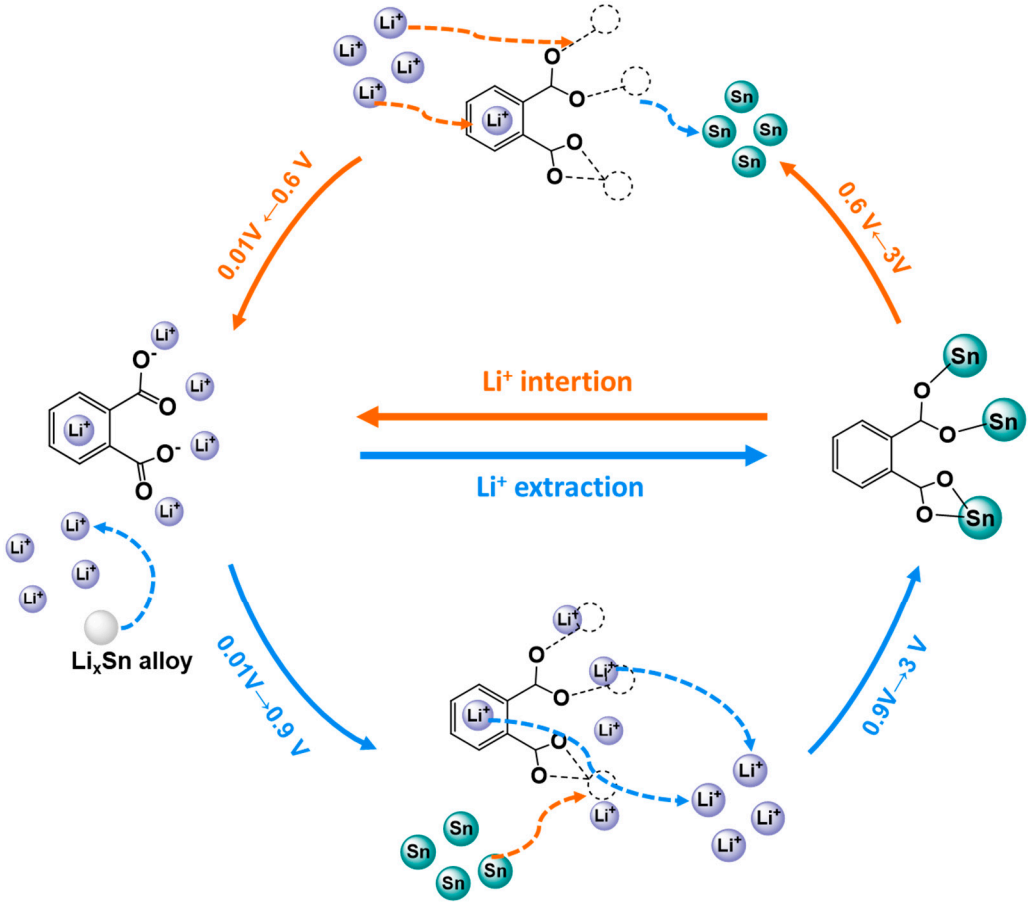

Figure 6. The lithium storage mechanism between the organic ligand and the Sn center (Ref. [96]).

MOF-based materials can also serve as functional separators to promote the Li^+ transport kinetics between the solid-state electrolyte and the electrode materials in lithium SSBs. An MOF-coated separator has been prepared by using Zr-based UiO-66-NH_2 and conventional commercial polypropylene. The grafted NH_2 group in the channels of UiO-66-NH_2 forms hydrogen bonds with the electrolyte PF_6^- anions promoting the Li^+ transport. It was found that the Li dendrite growth can be controlled in order to increase the ionic conductivity [97].

Another functional separator has been fabricated by modifying GF with UiO-66-NH_2 nanoparticles. The incorporation of UiO-66-NH_2 with OMs in the GF membrane anchors the ClO_4^- electrolyte enhancing the transport of Li^+ ions. Under high current density, this MOF-functionalized nanocomposite separator overcomes the Li metal anode issues as the large overpotential, dendrite penetration and low Coulombic efficiency [98–100]. The areal capacity of cells containing this MOF-functionalized nanocomposite was 3mA h cm^{-2} at the 1000 cycle, which is 74% of the value at second cycle [101].

A solid-state electrolyte has been prepared by fabrication of a 3D interconnected UiO-66 network via electrospinning and then backfilled with polymers (polyacrylonitrile (PAN), poly(ethyleneoxide) (PEO)) and lithium bis(trifluoromethane)sulfonimide (LiTFSI). The enhanced mechanical strength and uniform deposition of Li^+ by using the PAN/PEO-LiTFSI-based 3D-MOF effectively inhibits the growth of lithium dendrites as well as provides an ongoing route for Li^+ fast transport that increases the ionic conductivity [102].

In the promising high energy density (2600 mWh g^{-1}) and high theoretical capacity (1675 mAh g^{-1}) lithium–sulfur batteries severe self-discharge, insufficient capacity retention, limited charge–discharge coulombic efficiency associated with lithium polysulfides Li_2S_x formation and finally redox shuttle process are the most important limitations for their practical applications [103]. Different triphenylene-based 2D MOFs have been inves-

tigated as cathode host for Li-S batteries. 2D honeycomb MOFs have been obtained by using three different metal ions (Cu, Ni, and Co) and the hexasubstituted triphenylene linkers 2,3,6,7,10,11-hexaiminotriphenylene (HITP), 2,3,6,7,10,11-hexahydroxytriphenylene (HOTP) and triphenylene-2,3,6,7,10,11-hexathiol (THT). A study of their structural and electronic features together with an analysis of the catalytic activity showed the superior anchoring efficiency of $Co_3(THT)_2$ (−1.40 to −2.68 eV) due to the synergetic effect of functional groups (O/S) and Co. In addition, feasibly low energy barriers of 0.68 eV for Li^+ diffusion and 1.06 eV for Li_2S decomposition, and a small Gibbs free energy of 0.68 eV for Li polysulfide reduction and a moderately low Li_2S decomposition barrier (1.06 eV) contribute to achieving high performance Li–S batteries [104].

To suppress the shuttle effect (i.e., dissolution of polysulfide in organic solvents), an additional binding site has been incorporated introducing sulfiphilic metal ions (Cu^{2+}) into MIL-53(Al) MOF. The Cu^{2+} ions have high-binding energy to S_x^{-2}. By effectively anchoring copper to polysulfides Li_2S_x the polysulfide was immobilized and the dissolution suppressed. The bimetallic sulfur-loaded electrode material (Al/Cu-MOF-S) delivered a high-initial capacity of 974.2 mAh g^{-1} at 0.1 C [105].

The mesoporous $ZnMnO_3/C$ derived from MOF-5(Mn) and employed as anode material has contributed to high-performance Li-ion storage (specific capacities of 1500, after 293 cycles and 460 mA h g^{-1} after 500 cycles, respectively) [106].

A selenide composite has been synthesized on a graphene oxide-supported Ni-MOF. $NiSe_2$ nanoparticles in the octahedral MOF-derived rGO-$NiSe_2$ adsorb polysulfides and catalyzed their redox reaction suppressing the shuttle effect. The battery with an rGO-$NiSe_2$-modified separator yields a high initial capacity of 1356.5 mAh g^{-1} 0.2 C and achieves a low-capacity decay rate of 0.079% per cycle during 500 cycles of operation at 1 C [107].

The Zn@NPC-CeO_{2-n} composite has been demonstrated to be an efficient sulfur host for lithium-sulfur batteries. The catalytic effect of CeO_2 nanoparticles facilitates the conversion of polysulfides and improves the battery reaction kinetics [108]. The calcination of ZIF-8 meant that a high porous carbon materials Zn@NPC was able to provide effective physical adsorption of polysulfides. The specific discharge capacity of the battery was 569.3 mA h/g with 88% capacity retention after 200 cycles at 2 C [109].

An MOF-sulfur copolymer CNT@UiO-66-V-S has been designed as a cathode in lithium sulfur batteries to accelerate the redox kinetics and mitigate the shuttle effect of LiS_x. CNT@UiO-66-V-S has been obtained by copolymerization of sulfur with the vinyl functionalized UiO-66. The cathode delivers high specific capacity and cycling stability (initial specific capacity 853.2 mAh g^{-1} at 1 C and 609 mAh g^{-1} after 1000 cycles with a decay rate of 0.028% per cycle). However, severe shuttle effect and rapid loss of active materials inside the battery was observed after 310 cycles at 3 C [110].

The properties of the carbonized MOF-76(Gd) were investigated as it can serve as host for sulphur in cathode materials. The pores decrease the volumetric expansion of electrode during cycling, and effectively confine polysulphides inhibiting the shuttle effect. The cathode with carbonized MOF-76(Gd) exhibited an initial discharge capacity of 657.9 mAh g^{-1} after 200 cycles maintaining a capacity of 610.2 mAh g^{-1}, and high cycling stability [111].

The anchoring performance of LiS_x by transition-metals (TM)- and hexa-aminobenzene organic linker (HAB)-based 2D MOFs, has been investigated also by theoretical studies. (TM_3-$(HAB)_2$) complexes with a porphyrin-like structure have a single TM atom in every unit cell. The study highlights a strong chemical interaction of V-MOF and Ru-MOF with S_8, with larger adsorption energy and shorter van der Waals radii. Moreover, DFT calculations indicate that the lithiation process on V-MOF exhibited a nearly constant of about 1.92 V to 1.95 V with formation of $Li_{16}S_8$ clusters, and the theoretical energy density could reach up to 1469 Wh kg^{-1} considering the adsorption on both sides of V-MOF [112].

4.2. Na-Ion Batteries

SIBs represent a competitive system to replace LIBs, primarily for the lowest cost of abundant sodium-based sources [113]. The Na^+ ion has a larger ionic radius and higher

mass than Li^+, which affects the ionic transport kinetics and produces large structural changes in the electrode materials during sodiation/desodiation cycles. Low-rate capability, inferior cycling stability and relatively low discharge capacity are the critical issues in SIBs, the low initial Coulombic efficiency of the anode being the severe impediment limiting the energy density of sodium ion full battery [114]. However, the initial capacity loss of anodic material can be ascribed to the irreversible decomposition of the electrolyte, poor reversibility of sodiation/desodiation cycles, trap effect of defects and surface functional groups for Na^+ ion, and other side reactions [115]. Some effective strategies like electrolyte optimization, nanostructure and surface engineering of electrode materials, morphology tuning, and binder optimization have a great effect on reducing the initial capacity loss and improving the low initial Coulombic anode efficiency [116].

In order to obtain an advanced anode material for SIBs exhibiting excellent electrochemical performance, several classes of compounds have been investigated as anode and cathode, such as carbon-based materials [117], layered oxides, alloying-type materials [118] and transition-metal chalcogenides [119] In high-performance batteries, MOFs are promising candidates as electrode material, especially for low volume change, fast ions diffusion, high capacity, and energy density. However, poor electric conductivity and low energy density limit their general use in energy storage devices [120].

Electrochemically active 2D π-d conjugated MOFs, formed by planar conjugated organic ligands and square-planar metal nodes, are promising anode materials in SIBs. They promote the delocalization of electrons and provide adequate channel dimensions for rapid transmission of metal ions [121,122]. Two species have been built by using conjugated hexa-azatrinaphthylene hexa-hydroxyl (HATN-6OH) and hexa-2-ethylhexyl 2-mercaptoacetate (HATN-6SR) ligands, which are highly symmetric polycyclic aromatic heterocycles with rich redox-active C=N groups. In HATN-OCu (X = O or S) the synergic effect of a dual-redox site (C=N group and $[CuX_4]$ unit), exhibits impressive reversible capacity (500 mAh g^{-1} at 0.1 A g^{-1}) and high-rate performance (151 mAh g^{-1} at 5 A g^{-1}). In these 2D honeycomb-like π-d conjugated MOFs, the C=N group allows multielectron reactions achieving the reversible storage of Na^+ while the $[CuX_4]$ unit undergoes two consecutive reversible single-electron redox [123].

Thermal treatment of an MOF based on Co and 4,4′-biphenyldicarboxylate (Cobpdc-400) generates a phase transformation process in which the coordination number of cobalt ions is changed from six to four. This anode material displays much higher specific desodiation capacity (Figure 7), in which more sodium ions are inserted into the sp^2 carbon of benzene rings, delivering a reversible capacity of 413 mA h g^{-1} [124].

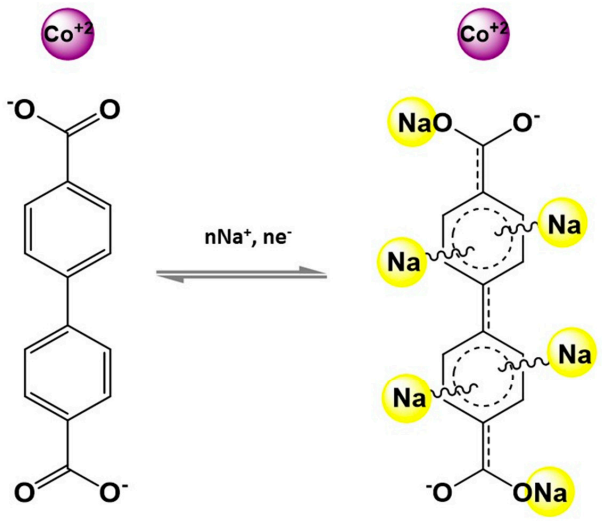

Figure 7. Proposed mechanism of sodiation of sp^2 carbon in benzene rings of Cobpdc-400. Adapted from [124].

A Mo-MOF has been used as sacrificial template to obtain MoO_2/NC micro rods covered with $MoTe_2$ nanosheets ($MoTe_2$@MoO_2/NC). The MoO_2 core enhances the electron transport rate, reducing the ion diffusion path. The doping of C and N increases the electrical conductivity ensuring the integrity of the structure. $MoTe_2$@MoO_2/NC demonstrates a high electrochemical performance with high capacity (~463.9 mAh g^{-1}) and fast-charge discharge ability (~294.7, and 258.3 mAh g^{-1} at 5, and 10 A g^{-1}, respectively) [125].

$CoSe_2$ is a potential alternative candidate to SIBs due to its outstanding sodium storage property. Nevertheless, its huge volume variation and sluggish diffusion kinetics lead to poor cycling stability and rate capability. $CoSe_2$-based anodes were fabricated via a selenization process, with ZIF-67 acting as template, anchored on MWCNTs ($CoSe_2$@NC/MWCNTs). The interconnected MWCNTs enhance the electronic conductivity and the ion/electron-transfer efficiency and suppresses the aggregation of $CoSe_2$ ensuring structural stability. By using it as SIBs anode a cycling performance of 441.2 mA h g^{-1} at 0.2 A g^{-1} (with the capacity retention of 92.0% over 100 cycles) and a rate performance of 227.4 mA hg^{-1} were displayed [126].

Core-shell $CoSe_2$/NC NPs embedded in 1D porous N-doped carbon nanotubes ($CoSe_2$/NC@NCNTs) have been synthesized. The rod-like cobalt-nitrilotriacetic acid (Co-NTA) MOF precursors were wrapped by polydopamine (PDA) shell via surface polymerization procedure (Co-NTA@PDA). Then, Co-NTA@PDA nanorods were annealed into the peapod-like Co/NC@NCNTs nanorods, and subsequently undergo the selenization process. The 1D porous $CoSe_2$/NC@NCNTs nanorods optimized in an electrode material showed sodium storage performance, good rate capability (386.3 mAh g^{-1} at 10.0 A g^{-1}) and high cycling stability (394.2 mAh g^{-1} up to 4500 loops at 5.0 A g^{-1}) [127].

A core-shell structure of Ni-ZIF-67@ZIF-8 has been carbonized and selenizated to form the Ni_3Se_4@$CoSe_2$@C/CNTs hierarchical structure in which Ni_3Se_4@CoS_{e2} nanocrystals were uniformly dispersed into the 3D carbon framework structure/carbon nanotubes networks. This conductive carbon shell/carbon nanotubes network enabled ultrafast Na-ion diffusion kinetics and when used as SIBs anode materials delivered an outstanding rate capacity of 206 mA h g^{-1} at 3A g^{-1} and steady cycle life after 600 cycles at 1 A g^{-1} [128].

The core-shell structure and the presence of biselenide components improve the conductivity as well as prevent the aggregation and volume expansion of the active material during the cycling. Indeed, in nickel-cobalt selenide@nitrogen-doped carbon (NiCoSe@NC) core-shell structures, a good mitigation of the volume expansion was observed during cycling. In a SIB employing $Na_3V_2(PO_4)_3$/C, a capacity of 177 mAh g^{-1} is maintained after 100 cycles (at 1 A g^{-1}) [129].

$Co_{0.85}$Se@carbon nanotubes grown on the surface of carbon microplates ($Co_{0.85}$Se@CNT-CP) have been prepared from ZIF-67 by a simple pyrolysis-selenization strategy. A 3D hierarchical structure with $Co_{0.85}$Se nanoparticles encapsulated in the top of CTNs showed steady cycle stability and discharge capacity of 306 mA h g^{-1} after 800 cycles at 2 A g^{-1}. These composites also showed a good rate capability of 222.5 mA h g^{-1} at 5 A g^{-1} [130].

A Co_3O_4-based carbon nanofiber composite (Co_3O_4@CNF) has been directly employed as a binder-free anode for SIB and has displayed a reversible capacity of 380 mAh g^{-1} for 150 cycles at 100 mA g^{-1}, high-rate capability, and long cycling stability (it maintains 129 mAh g^{-1} after 500 cycles at a high current density of 3.2 A g^{-1}). The Co_3O_4@CNF has been obtained by using ZIF-67/CO^+ particles prepared by an in situ growth method, stringed on the heteroatoms-doped carbon nanofibers through electrospinning method to form hierarchical carbon nanofiber, subsequently carbonized and oxidized [131].

A multi-layered yolk-shell $CoSe_2$ nano-dodecahedron has been synthesized by step-by-step epitaxial growth of ZIF-67 and ZIF-8 and post carbonization/selenization processes. The resulting three-layer hollow yolk-shell structure maintains its features during charging and discharging and the SIB electrode showed a discharge capacity of 352.9 mAh g^{-1} at the current density of 1 A g^{-1} providing a large number of active sites for the insertion of sodium ion [132].

Hierarchical carbon-encapsulated yolk-shell nickel spheres (Ni_2P/C, NiS_2/C and $NiSe_2/C$) have been synthesized from Ni-MOF by hydrothermal and anion exchange strategy. The yolk-shell structure can provide large contact areas electrode materials/electrolyte, and effective transport paths for Na^+/electrons, and, maintaining the structural integrity the Ni_2P/C anode achieved high initial specific capacity (3222.1/1979.3 mAh g^{-1}) and reversible capacity of 765.4 mAh g^{-1} after 110 cycles [133].

Copper chalcogenides-carbon composites ($Cu_{1.8}S$@C and $Cu_{2-x}Se$@C) have been synthesized by a sulfidation/selenization strategy carried out on HKUST-1 derivatives. When carbon-coated $Na_3V_2(PO_4)_3$ (NVP/C) positive electrodes have been employed as anode materials, $Cu_{1.8}S$@C and $Cu_{2-x}Se$@C exhibited high specific capacities of 504 mAh g^{-1} and 317 mAh g^{-1} at 0.1 A g^{-1}, respectively. The carbon-coated $Na_3V_2(PO_4)_3$ (NVP/C) cathode materials in the sodium-metal cell, Na $Cu_{2-x}Se$@C and Na $Cu_{1.8}S$@C cells also exhibit promising performances. Notably, a $Cu_{2-x}Se$ @C NVP/C cell delivers a specific capacity of 73 mAh g^{-1} at 1.2 A g^{-1}, good cycling stability (capacity retention of 85% after 500 cycles at 0.12 A g^{-1}) with Coulombic efficiency of 100% [134].

POMs are a class of metal oxide cluster anions that can be employed as sodium-ion storage materials and have interesting features as reversible multielectron redox properties and high ionic conductivity [135]. To avoid loss and aggregation of POMs in SIBs, a PMo12/MOF/GO composite was fabricated using three isomeric iron-based MOFs (MIL-101, MIL-53, and MIL-88B) with different topologies, pore sizes and with a "breathing effect". The sodium storage performance is relevant in PMo12/MIL-88B/GO. The pore geometry of MIL-88B facilitates Na^+ diffusion, leading to the favored energetic kinetics and surface-control capacity. PMo12/MIL-88B/GO exhibited the highest reversible discharge capacity of 214.2 mAh g^{-1} for 600 cycles at 2.0 A g^{-1} [136].

CoNiZnS/C, an SIBs anode material, has been prepared by solid sulfidation of a tri-metal-organic framework (Co-Ni-Zn MOF). The special microsphere structure of CoNiZnS/C presents abundant active sites and defects for storing sodium ions and rich voids to alleviate the volumetric strains. The composite has demonstrated high initial Coulombic efficiency (96.52% at 0.1 A g^{-1}), good cycling stability (410.7 mA h g^{-1} at the 960th cycle at 2.0 A g^{-1}) and excellent rate performance (477.0 mA h g^{-1} at 5.0 A g^{-1}). [137].

Layered transition-metal oxide (Na_xMnO_2) cathodes have been fabricated starting from the pure $Na[Mn(HCOO)_3]$ MOF via ultrafast calcination process. The P2-phase layered sodium manganese oxide (P2-Na_xMnO_2) has been obtained with open prismatic paths in which Na^+ ions can diffuse between metal layers. Excellent sodium storage performance, with a high specific capacity of 212 mA h g^{-1} and a cycling performance has been achieved [138].

4.3. Other Metal-Ion, Metal Air Batteries

Metal-air batteries represent a cost-effective and environmentally friendly technology in the large field of energy storage devices. The energy density and the specific capacity of a metal–air battery is higher than that of conventional rechargeable batteries, making them a suitable candidate for use in electric vehicles. A metal-air battery consists of a metal anode, an external cathode in ambient and a metal salt electrolyte. During discharging and charging processes the ORR and OER take place at the ambient air cathode, while the metal anode is oxidized. However, the slow kinetics of ORR and OER affect the charge/discharge capability of metal-air batteries. To improve capability of metal-air-batteries, the electrocatalysts should have high efficiency with activities in both reactions.

In general, noble metal-based electrocatalysts have been used to enhance the sluggish of ORR and OER reactions in the discharging and charging processes, but high cost and poor stability are the main disadvantages. Recently, porous MOFs with tunable metal cations have demonstrated to be suitable platforms to enhance catalytic performance in both ORR and OER reactions.

The hierarchical porous FeNP@Fe-N-C electrocatalyst was obtained through one step pyrolysis of the Fe-doped ZIF-8. The Fe-N_4 sites were dispersed in nanotube walls

whereas iron metallic nanoparticles (FeNP) were encapsulated in the nanotubes. The micro and mesoporous FeNP@Fe-N-C catalyst decorated with Fe-N_4 sites and Fe nanoparticles boosted the adsorption, activation, and conversion of oxygen during ORR)/OER. Rechargeable zinc-air battery based on FeNP@Fe-N-C catalyst demonstrated high open-circuit voltage of 1.45 V, and high-power density of 106.5 mW cm^{-2} with a stable cycling performance [139].

A lithium-air battery employing a cobalt@porous carbon composite (Co@C) obtained by facile annealing of a Co/Zn bimetallic MOF, exhibits very good performances due to the disseminated cobalt nanoparticles in the C matrix and to the fast diffusion of both Li^+ and O_2 owing the suitable pore-distribution [140].

The double-sandwich-like structure MOF-derived carbon/manganese silicate/reduced graphene oxide/manganese silicate/MOF-derived carbon has been used as cathode material for aqueous rechargeable Zn-ion batteries. This integrated system not only shows an improved electronic conduction but also displays Zn^{2+} storing capacity [141].

A 3D carbon matrix was fabricated through pyrolysis of Co ions encapsulated in ZIF-8 intercalating GO sheets. The unusual N-doped CNTs architecture allowed the additional exposure of active sites and the synergistic interaction between metal nanoparticles and CNTs. The Zn/Co-NGC exhibited methanol resistance in alkaline and acidic solution with ORR performance close to benchmark Pt/C catalyst ($E_{1/2}$ = 0.80V in 0.1 mol L^{-1} KOH; $E_{1/2}$ = 0.75 V in 0.5 mol L^{-1} H_2SO_4) in 0.1 mol L^{-1} KOH solution ($E_{1/2}$ = 0.83 V) and 0.5 mol L^{-1} H_2SO_4 electrolyte ($E_{1/2}$ = 0.73 V). The highest power density for a zinc-air battery assembled with Zn/Co-NGC was 90 mW cm^{-2}. The batteries also showed excellent charge/discharge cycle stability [142].

The high activity and structural stability of perovskite oxides make them promising candidates for efficient bifunctional oxygen electrocatalysis [143]. MOF-derived $PrCoO_3/Co_3O_4$ nanocages (PCO/Co_3O_4 NCs) were prepared in situ by decoration of ZIF-67 with Pr precursor, followed by a sintering process. The core–shell PCO/Co_3O_4NCs catalyst with perovskite/spinel heterointerface exhibited a low overpotential of 371 mV in 0.1 M KOH at 10 mA cm^{-2} for OER and a remarkable reduction of half-wave potential of 0.72 V for ORR. When the catalyst was assembled in a zinc-air battery, a power density of 182 mW cm^{-2} and long-term operation of 185 mW cm^{-2} has been observed [144].

5. Supercapacitors

Since the first employment of several Co-based MOFs by Diaz [145] and Lee [146] MOFs have been also extensively investigated as electrode materials in supercapacitors. However, these species showed poor electrochemical performances, so different strategies have been more recently proposed as the composition of MOFs with conductive matrix or the use of conjugated ligands [147,148]. Additionally, hybrid materials based on conductive 2D MOFs nanosheets/rGO heterostructure have been demonstrated to be promising materials for next-generation supercapacitors [149]. A recent review reported the results obtained with pillar-layered MOFs having both interpenetrated and non-interpenetrated topologies. Several perspectives have been also proposed as the accommodation of molecules with more redox centers into the pore in non-penetrating MOFs, or the use of large p-conjugated systems, or also the construction of 3D conductive MOFs which endows omnidirectional ion-transport path for the charge-discharge process [150]. The capacitive performance and the structure property relationships of a series of both MOFs and COFs have also been reviewed and related to their structural stability and to the presence of redox-active sites and high electronic conductivity, fundamental for their use in high-performance supercapacitors electrodes [151].

Zn-based MOFs (CZMOF) carbonized at 1000 °C have been employed as materials for supercapacitor electrodes exhibiting the highest specific capacitance reported to date for Zn MOF-derived electrodes (Figure 8). Their applicability has been tested in non-aqueous electrolytes [152].

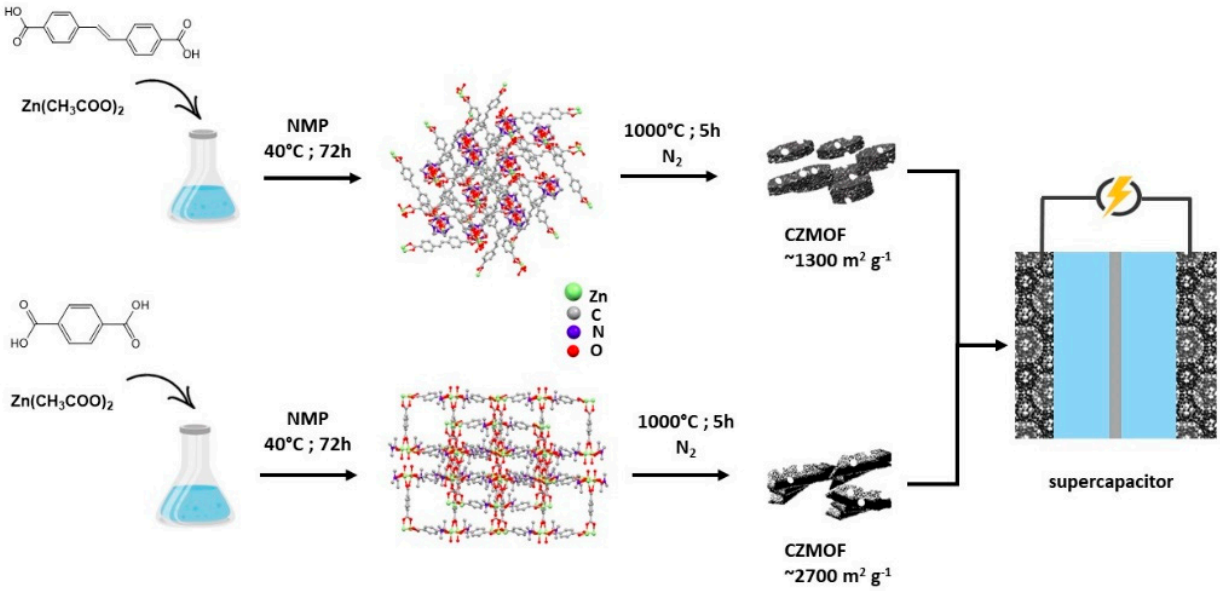

Figure 8. Scheme of the synthesis of Zn-based MOF-derived porous CZMOF employed as electrode material in a supercapacitor (Ref. [152]).

Conductive MOF@metal oxide micro-nanocomposites have been prepared via a facile self-assembly. It has been reported an enhancement of the electrical conductivity for these micro-nanocrystallized compounds without ions transfer efficiency decreasing. It has been found that specific facet exposure and small sizes are significant to obtain high capacitance [153].

The hybrid nanomaterial obtained by $Ag_5[BW_{12}O_{40}]$ and $Mn_3(BTC)_2(H_2O)_6$ and characterized by a core-shell construction, used in a three-electrode system with a nickel foam as collector, showed a specific capacitance of 198.09 F g^{-1} at a current density of 1 A g^{-1}. Also the $Ag_5[BW_{12}O_{40}]$@Ag-BTC core-shell hybrid showed a significant capacitance and a power density of 496 W kg^{-1} [154].

A mesoporous material has been prepared by injection of a POM cluster into an MOF with the aim to insert more additional redox centers. $[Co_3Mo_7O_{24}]$@Ag-BTC, prepared by a simple grinding method, showed a high specific capacitance (260.7 F g^{-1}) and high capacitance retention (99.8% after 5000 cycles) [155].

The dual-ligand and hard soft acid-base strategies have been employed to produce a 3D-pillared-layer MOF nanocrystal based on Ni, thiophene-carboxylate and bipyridine in the form of 1D nanofibers, 2D nanosheets and 3D aggregates, the 2D nanosheets showing the larger specific capacitance due to the shorter ion diffusion length and strong interaction between the two ligands [156].

A microporous two-dimensional Ni-MOF highly scalable and thermodynamically stable over a wide pH range (2–10) and GO were employed to produce a composite showing high specific capacitance value. The presence of ligands having delocalized p-electrons on the MOFs and the integration with the conducting GO significantly boost the conducting properties of the material [157].

An MOF based on Ni and hexahydroxybenzene combined with $Ni(OH)_2$ nanosheets produced a series of Ni-MOF@$Ni(OH)_2$ nanoarrays which show a high electrical conductivity and ionic transfer efficiency. When MOF@$Ni(OH)_2$ was assembled as positive electrode in an aqueous asymmetric supercapacitor a capacitance retention of 98% after 5000 cycles was found [158]. It is well known that hybrid electrode material generally shows good electrochemical activity with rapid ions diffusion [159]. Asymmetric supercapacitors have been assembled using CuMOF/rGO as negative electrode and V_2O_5/rGO as positive. They display high specific capacitance and good cyclability [160]. Vanadium MOFs have been also reviewed together their application in energy storage [161]. A special focus has been

given to MIL-47, easy to synthesize and useful as electrode material for supercapacitors. It has been found that MIL-47 is able to promote a good ions diffusion and to exhibit a maximum specific capacitance of 572.1 F g^{-1} at current density of 0.5 A g^{-1} [162].

6. Water Splitting Reaction

Water splitting is an eco-friendly technology useful to produce alternative and sustainable energy, as it is a way to produce hydrogen by electrochemical, chemo-catalytic or photocatalytic methods. It consists of two different reactions: the HER, H_2 evolving at cathode, and the OER, both H_2 and O_2 evolving at an anodic surface. HER carried out in acidic or basic media is today considered one of the most important methods because it yields pure hydrogen, however the kinetics of this reactions is sluggish and is fundamental to use effective catalysts. Several metals have been investigated as HER electrocatalysts, in most of the cases they are precious metals or Ru/Ir materials, however their availability, stability and high cost prevented further application. MOFs, due to their porosity, large surface area and stability can be considered ideal candidates as electrocatalyst for the water splitting process. They can be chosen not only because they can replace expensive metal-based catalysts, but also because they are able to lower the overpotential during the HER and to increase the kinetics of the reaction [163]. The modulation of MOF structure, for example in the form of hybrids, is the better way to make easy the electron transfer and to increase the catalyst conductivity [164]. Electrolytic cells with MOF-modified electrodes characterized by a significant catalytic activity, together with novel strategies, have recently been reported to improve the conductivity [165].

The photochemical and photoelectrochemical capabilities of MOF and MOF-derived materials and their tuning by modification in the bandgap, surface area current density and overpotential with appropriate choice of organic ligands and metal centers has been well described in 2020 [166], whereas the most important strategies to produce MOF-based composites by using different organic ligand, quantum dots and carbon-based derivatives, as also the production of thin-film photoelectrodes for photoelectrochemical water splitting by merging MOF layers with semiconductors, have been described in a recent review [167]. The heterogeneity of mixed metal-MOFs, prepared by introducing different metal ions or different organic linkers in homogenous MOF systems seems also very relevant to improve the MOFs performance as photocatalyst for H_2 evolution from water splitting reaction, as recently described in a review [168]. MOFs can be also employed as template for the synthesis of highly reactive transition metal phosphides very suitable candidates for efficient electrocatalytic water splitting [169]. The relation between the performance and the structure of the MOFs has been also evidenced together with a perspective on the future industrial applications. MOF-based electrocatalysts for water splitting and CO_2 reduction reaction have been also reported [170].

A fully p-conjugated, bidimensional and conductive MOF has been obtained from the reaction of nickel salt with benzenehexathiol, that upon deposition on the photocatalyst $SrTiO_3$:Al in the presence of CoO_x as O_2 evolution cocatalyst, demonstrates long-term overall one-step water splitting. It has been found that while the use of Pt as HER cocatalyst promotes non only the forward reaction, i.e., the H_2 evolution, but also the unfavorable backward H_2O restoration, the Ni MOF promotes only the forward reaction [171]. The ligand choice is extremely important: the replacement of the ligand in NH_2-MIL-125 by 1,4-dicarboxybenzene can improve the charge transfer dynamic by preserving the MOF light adsorption and giving a higher H_2 production rate [172]. Co(II) based MOFs are very interesting as Co has multiple valence states and is also abundant. For this reason, Co(II) MOFs can be employed as an electrocatalyst in overall water splitting. Their combination with carbon-based hybrid materials can overcome several problems, i.e., the relative insulation of Co-MOF and the not-variability of the carbon-based materials. On the other hand, when the MOFs and the carbon materials are simultaneously employed synergistic effect have been observed, i.e., the increasing of the surface rate and the acceleration of the electron transfer rates. All the results collected with these systems are summarized in a recent

review [173]. The OER potential is very high and affects the efficiency of water splitting, so catalysts with high performance are required as the hollow Co-ferrocene-MOF derived phosphides that thanks to enriched P,O vacancies and unique morphology synergistic effect exhibit a high conductivity [174].

The integration of an Fe amorphous interface with a Co-MOF generates an improvement of the catalytic performance toward OER and HER with significant perspectives in development of electrocatalysts for water splitting (Figure 9) [175].

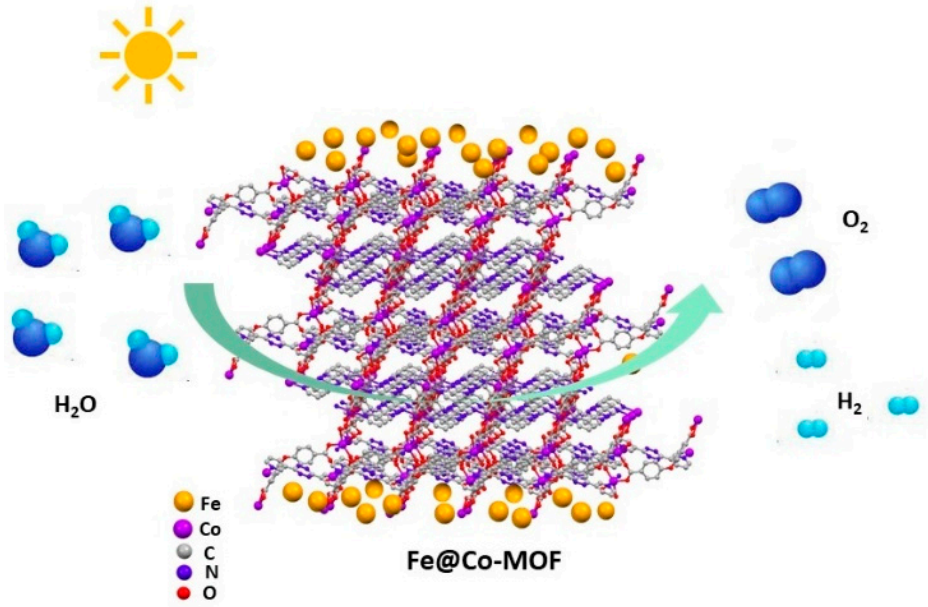

Figure 9. Synthesis of an amorphous material Fe@Co-MOF obtained from a crystalline Co-MOF and amorphous Fe interface (Ref. [175]).

As the hematite is also a promising photoanode for photoelectrochemical water splitting, an ultrathin ZIF-67 layer was deposited on the surface of Sn/Ti co-doped a-Fe_2O_3 by solvothermal methods. The photocurrent intensity was four-fold that of the pristine hematite [176]. A nickel-based MOF based on 1,3,6,8-tetrakis(p-benzoate)pyrene ligand and its exfoliated nanobelts show electron transfer from the ligand to the Ni-O cluster. On this catalytic center the water splitting reaction can be performed to produce hydrogen without necessity of cocatalyst [177]. A NiFe-MOF has been prepared and used to modify $BiVO_4$ yielding a novel composite photoanode. The photocurrent density, the stability, the incident photon-current conversion efficiency and both the injection and separation efficiency of the photoanode have been significantly improved [178]. A bidimensional MOF-derived mesoporous CoS_2 nanoarray coupled with FeS_2@MoS_2 exhibit high electrocatalytic activity toward both HER and OER. It has been reported that the greater efficiency, with respect to other systems reported in literature, is due to the abundant interfaces, multi-metallic active centers and mesoporous nanostructures [179].

It has been reported that UiO-66/MoS_2 hybrid is a promising non-expensive electrocatalyst for overall water-splitting reaction and that the synthetic methods employed to obtain this hybrid play a role in the formation of a peculiar structure determining the activity and catalytic performances [180].

Highly efficient OER electrocatalysts Co-based have been obtained from a two-dimensional MOF based on a sulfur-containing linker. The sulfur source is fundamental to reduce waste as well as to disperse Co [181].

It is very important the stability of the materials in water: for this reason, for example, hierarchical structures have been generated by inserting anions as MoO_4^{2-} in MiL-53 (NiFe) MOF. The electrode NiFeMo-MOF/NF demonstrated an efficient overall water splitting [182]. A vanadium doped Ni-MOF, obtained by a two-step solvothermal methods,

demonstrated a greater efficiency toward OER with respect to the corresponding single Ni-MOF and RuO_2 catalysts [183].

A hybrid catalyst based on Mo_2C and UiO-66 obtained by solvothermal methods showed a very good catalytic performance in both HER and OER. A synergistic effect has been indicated as responsible of a hydrogen adsorption energy decrease offering excellent catalytic activity in alkaline medium for water splitting [184]. MX-ene decorated with carboxyl groups are connected to UiO-66-NH_2(Zr/Ti). The carboxylate not only can help to generate a hybrid between MOF and MX-ene but can also promote the electron transfer from the two materials and interact with the oxygen from water promoting its dissociation into OH and H [185].

An In-based MOF prepared by interaction of a functional tetracarboxylic acid with a In^{III} center and connected to a single-metal-node-based porous three-dimensional pts net has been investigated as photocatalyst for H_2 production from water splitting and demonstrated to be very efficient with a suitable band gap [186].

The introduction of defects and in situ oxidation of the electrocatalysts can yield heterostructures active for OER and HER by boosting their sluggish kinetics. This has been clearly demonstrated by the alkaline water splitting enhancement by the heterostructure MOF-derived Fe-Co-oxide/Co@NC-mNS [187].

Calcination of a Cd-MOF and loading CdS through ionic layer adsorption produced a porous Cds/CdO-M heterojunction photoanode able to promote the separation and transfer of photogenerated electron-hole in the photoelectrochemical water splitting [188].

Fe-based MOFs continue to attract attention as water splitting electrocatalysts due to their low toxicity and cost. A series of Fe-MOF/Au composites has been grown in situ on Fe foam, the latter acting as conductive substrate and self-sacrificing template. It is possible to adjust the electronic structure of the obtained nanorods, which exhibit not only overall water splitting but also enhanced conductivity, by tailoring the electrodeposition time [189].

An MOF-derived S-doped NiFeP structure has been realized by a one-step procedure. It has been found that both OER and HER performances of the NiFeP catalyst are strongly improved upon partial replacement of P by S [190].

A pore-space-partition strategy has been also applied for water splitting, by producing a series of ultra-stable electrocatalysts based on a vanadium trimetallic building cluster M_2V and pristine MOFs. This family of electrocatalysts is able to yield a current density greater than that reported for commercial IrO_2//Pt/C couple [191].

A nanosheet array of a Ni/Co MOF grown on a Ni foam substrate, also modified with CoO and obtained by solvothermal techniques showed efficient water splitting due to the high surface area and low resistance. A high electrocatalytic performance in alkaline medium has been reported and attributed to synergistic effects of Ni/Co MOF and Co/Ni foam [192]. A Ni-MOF containing carboxylate and bipyridine ligands has been demonstrated useful for ultrafast and selective sensing of explosives and suitable as a photoanode material for visible-light-driven water splitting (photoelectrochemical hydrogen evolution) [193].

The Zn-centered MOF ZIF-8 has been employed as precursor to produce Ru-based electrocatalysts (ultrathin Ru and Ru_2O 3D macropore N-doped carbon framework) which show good electroconductivity, excellent electron/mass transport and overall water splitting as a consequence of their structural features, N doping and abundant catalytic sites [194].

Ultra-low Ru doped MOF-derived hollow nanorods has also been prepared by $NaBH_4$ reduction strategy. This material showed excellent OER performance, good overall water splitting activity and long-term stability [195]. A nitrogen-doped mesoporous carbon, trifunctional catalyst has been prepared by pyrolysis of two Co-MOFs, one linear coordination polymer and one complex and investigated for OER and HER in alkaline electrolyzers and also demonstrated catalytic activity towards ORR [196].

7. Conclusions and Future Perspectives

The strong dependence of modern society on fossil fuels produces several environmental problems and an energy request that we are not able to satisfy with the actual reserves. For this reason, the fossil fuel limitations have pushed communities towards extensive development of renewable energy resources.

MOFs seem to constitute an important resource for possible application in energy conversion and storage devices. MOFs are advantageous for the installation of electron reservoirs for metal-ion battery electrodes and their porosity plays a role in modulating ion transport. MOFs are good candidates for enhancing proton conduction performances, for example the presence of defects or of donor ligands able to accept and release H^+ can improve the conductivity and give us a perspective material for fuel cells. MOFs can efficiently be employed in dye-sensitized solar cells and in photoelectrochemical cells, the interaction of MOFs with perovskite precursors often being able to produce an enhancement of the efficiency of photovoltaic devices.

Over the years batteries have evolved. Several MOFs have been successfully employed as both cathode and anode materials for Li- and Na-ion batteries and structural modifications have been proposed with the goal to obtain a better charging-discharging capacity, higher cyclic and structural stability [197–199]. LIBs based on a graphite anode and a transition metal oxide cathode reached their performance limits mainly due their instability and irreversibility. The use of MOFs as electrode material has allowed a better electrolyte penetration and ion transportation, and the introduction of electroactive sites. Even if their electrical conductivity continues to be the main limit, as it affects reaction kinetics and electron-rate transfer, electrodes based on MOFs can exhibit better cyclic performance: for example, MOFs presenting Lewis acidic and basic organic ligands show ability to sulfur storage and sulfide confinement in Li-S batteries. In Li-S batteries, the MOFs have been demonstrated useful to prevent dendrite formation and polysulfide shuttle.

Moreover, the stability of pristine MOF structure affects the cycling stability. Cycling performances of the electrode can be improved utilizing a multi-metal organic framework, through which the dimension change can be reduced during the continuous insertion/deintercalation of lithium/sodium ions. In addition, the presence of the nitrogen atoms in the organic ligands can be used as active sites for inserting ions and the strong coordination bonds formed by metal centers and nitrogen-organic ligands improve the stability MOFs structure.

MOF derivatives have been demonstrated to be performant in SIBs for sodium storage, for example reducing the Na adsorption energy by enhancing the nucleation and deposition of Na. MOFs and MOF composites showing high electrical conductivities and chemical stability have been directly used as bifunctional catalysts in Li-O_2 batteries, but the knowledge of their catalytic mechanisms is necessary in order to explore and find new MOF-derived cathode materials. The morphology and the structure of the materials employed in batteries are relevant for the Li^+ and Na^+ insertion, so new approaches to production of stable nanostructures will be important in the next years.

Recent progress outlines the use not only of MOFs in metal-air and metal-sulfur batteries but also in supercapacitors. The pH stability of MOFs as also their scalability fulfils the requirement of efficient electric double layer capacitance with long cyclic stability.

Finally, MOFs can be used as electrocatalysts in water splitting reaction. Useful strategies for the synthesis of catalysts, their challenge and their role in water splitting have been clearly evidenced. Selected examples of the different categories of application reported for MOF materials are listed in Table 1.

Table 1. Different categories of application of selected MOF materials.

Application		MOF	Typology	Ref.
Fuel Cells				
	PEMFC	ZIF-8	Precursor	[43]
		ZIF-8	Composite	[44]
		UiO-66	Composite	[46]
		BUT-77	Pristine	[47]
		MOF-5	Derivative	[49]
	DMFC	MIL-101-NH_2	Composite	[52]
Solar Cells				
	PSC	MIL-125(Ti)	Precursor	[57]
		Zr-MOF	Composite	[59]
	DSSC	MIL-101	Composite	[60]
Batteries				
	Li-ion Batteries	ZIF-62(Co)	Composite	[77]
		d-p conjugated Ni CPs	Composite	[81]
		ZiF-67	Composite	[89]
		MIL-125(Ti)	Precursor	[91]
		CAU-17	Precursor	[92]
		ZIF-8	Composite	[93]
		Sn-MOF	Pristine	[96]
		UiO-66-NH_2	Composite	[98–100]
		UiO-66	Composite	[111]
	Na-Ion Batteries	HATN-OCu	Pristine	[124]
		Cobpdc-400	Precursor	[125]
		Ni-ZIF-67	Precursor	[129]
		MIL-88B	Composite	[137]
Supercapacitors				
		AgBTC	Composite	[156]
		Ni-MOF	Composite	[159]
		MIL-47	Pristine	[163]
Water splitting				
		Co-Ferrocene	Composite	[179]
		UiO-66	Composite	[180]
		In-MOF	Pristine	[187]
		Cd-MOF	Precursor	[189]
		Ni-MOF	Pristine	[194]
		ZiF-8	Pristine	[195]
		Ru-MOF	Composite	[196]

Despite this great potential there is still much to investigate to produce effective applications of MOFs in electrochemical energy storage devices. For example, the impact of microstructure and particle morphology of MOFs and MOFs-derived materials on the capacity and rate performances is not yet fully understood. MOFs are in most of cases employed as simple supporting material and not for the essential role it could play. The conductivity of MOFs needs to be improved, this being the main problem for photo- and electro-chemical energy applications: the use of photosensitive organic ligands and metal centers that change oxidation states with relative ease could guarantee better performances. MOF composite materials are poorly studied as the ligand role in most of the hybrids explored to date. In addition, MOF hybridization and carbonization methods still need to be tuned and optimized. The design of new strategies and preparation methods of MOF composites and derivatives could be fundamental. The application conditions for a practical use should also be better set as the mechanisms of most of the processes need to be investigated and clarified. As the number of MOFs synthesized and investigated

increases, the perspective of pristine MOFs, MOF composites and MOF derivatives for energy applications will increase in the coming years.

Author Contributions: Conceptualization, C.P. and A.T.; methodology, C.P. and A.T.; writing—original draft preparation, C.P. and A.T.; writing—review and editing, C.P. and A.T; funding acquisition, C.P. All authors have read and agreed to the published version of the manuscript.

Funding: This research was funded by University of Camerino through a grant to AT.

Acknowledgments: University of Camerino is gratefully acknowledged.

Conflicts of Interest: The authors declare no conflict of interest.

Abbreviations

CNFs = carbon nanofibers; CNTs = carbon nanotubes; DMFC = direct methanol fuel cell; DSSC = dye sensitized solar cell; ECS = energy conversion and storage; GF = glass; GO = graphene oxide; HAGO = horizontally aligned graphene oxide; HER = hydrogen evolution reaction; LIBs = lithium-ion batteries; LiPS = lithium polysulfide; MOFs = metal organic frameworks; MX-ene = metal carbides; MWCNTs = multiwalled carbon nanotube networks; NPs = nanoparticles; NCNTs = N-doped carbon nanotubes; OER = oxygen evolution reaction; OMS = open metal sites; ORR = oxygen reduction reaction; PCMs = polyacrylate carboxyl microspheres; PECs = photoelectrochemical cells; PEM = proton exchange membrane; PEMFCs = polymer electrolyte membrane fuel cells; POMs = polyoxometalates; PSCs = perovskite solar cells; SACs = single atom catalyst; SIBs = sodium-ion Batteries; SSBs = solid-state batteries.

References

1. Lawson, H.D.; Walton, S.P.; Chan, C. Metal-Organic Frameworks for Drug Delivery: A Design Perspective. *ACS Appl. Mater. Interfaces* **2021**, *13*, 7004–7020. [CrossRef] [PubMed]
2. Rowsell, J.L.C.; Spencer, E.C.; Eckert, J.; Howard, J.A.K.; Yaghi, O.M. Gas adsorption sites in a large-pore metal-organic framework. *Science* **2005**, *309*, 1350–1354. [CrossRef] [PubMed]
3. Li, H.; Wang, K.; Sun, Y.; Lollar, C.T.; Li, J.; Zhou, H.C. Recent advances in gas storage and separation using metal–organic frameworks. *Mater. Today* **2018**, *21*, 108–121. [CrossRef]
4. Xia, W.; Mahmood, A.; Zou, R.; Xu, Q. Metal–organic frameworks and their derived nanostructures for electrochemical energy storage and conversion. *Energy Environ. Sci.* **2015**, *8*, 1837–1866. [CrossRef]
5. Furukawa, H.; Cordova, K.E.; Keeffe, M.O.; Yaghi, O.M. The Chemistry and Applications of Metal-Organic Frameworks The Chemistry and Applications of. *Science* **2013**, *341*, 1230444. [CrossRef]
6. Chen, T.; Chen, S.; Chen, Y.; Zhao, M.; Losic, D.; Zhang, S. Metal-organic frameworks containing solid-state electrolytes for lithium metal batteries and beyond. *Mater. Chem. Front.* **2021**, *5*, 1771–1794. [CrossRef]
7. Calbo, J.; Golomb, M.J.; Walsh, A. Redox-active metal–organic frameworks for energy conversion and storage. *J. Mater. Chem. A* **2019**, *7*, 16571–16597. [CrossRef]
8. Cheng, H.; Shapter, J.G.; Li, Y.; Gao, G. Recent progress of advanced anode materials of lithium-ion batteries. *J. Energy Chem.* **2021**, *57*, 451–468. [CrossRef]
9. Baumann, A.E.; Burns, D.A.; Liu, B.; Thoi, V.S. Metal-organic framework functionalization and design strategies for advanced electrochemical energy storage devices. *Commun. Chem.* **2019**, *2*, 86. [CrossRef]
10. Wu, H.B.; Lou, X.W. Metal-organic frameworks and their derived materials for electrochemical energy storage and conversion: Promises and challenges. *Sci. Adv.* **2017**, *3*, 1–16. [CrossRef]
11. Dědek, I.; Kupka, V.; Jakubec, P.; Šedajová, V.; Jayaramulu, K.; Otyepka, M. Metal-organic framework/conductive polymer hybrid materials for supercapacitors. *Appl. Mater. Today* **2022**, *26*, 101387. [CrossRef]
12. Nik Zaiman, N.F.H.; Shaari, N.; Harun, N.A.M. Developing metal-organic framework-based composite for innovative fuel cell application: An overview. *Int. J. Energy Res.* **2022**, *46*, 471–504. [CrossRef]
13. Zhang, Y.; Huang, Q.; Liu, J.; Zhou, J.-E.; Lin, X.; Zeb, A.; Chenna, R.; Reddy, K.; Xu, X. Recent advances in Fe-based metal–organic framework derivatives for battery applications. *Sustain. Energy Fuels* **2022**, *6*, 2665–2691. [CrossRef]
14. Wei, T.; Wang, Z.-M.; Zhang, Q.; Zhou, Y.; Sun, C.; Wang, M.; Liu, Y.; Qiu, X.-Y.; Xu, S.; Qin, S. Metal-Organic Frameworks-Based Solid-State Electrolytes for All Solid-State Lithium Metal Batteries: A Review. *CrystEngComm* **2022**, *2*, 5014–5030. [CrossRef]
15. Zhou, J.; Yang, Q.; Xie, Q.; Ou, H.; Lin, X.; Zeb, A.; Hu, L.; Wu, Y.; Ma, G. Recent progress in Co–based metal–organic framework derivatives for advanced batteries. *J. Mater. Sci. Technol.* **2022**, *96*, 262–284. [CrossRef]
16. Peng, Y.; Xu, J.; Xu, J.; Ma, J.; Bai, Y.; Cao, S.; Zhang, S.; Pang, H. Metal-organic framework (MOF) composites as promising materials for energy storage applications. *Adv. Colloid Interface Sci.* **2022**, *307*, 102732. [CrossRef]

17. Zeeshan, M.; Shahid, M. State of the art developments and prospects of metal–organic frameworks for energy applications. *Dalt. Trans.* **2022**, *51*, 1675–1723. [CrossRef]
18. Yan, J.; Liu, T.; Liu, X.; Yan, Y.; Huang, Y. Metal-organic framework-based materials for flexible supercapacitor application. *Coord. Chem. Rev.* **2022**, *452*, 214300. [CrossRef]
19. Zhou, D.; Wu, T.; Xiao, Z. Self-supported metal-organic framework nanoarrays for alkali metal ion batteries. *J. Alloys Compd.* **2022**, *894*, 162415. [CrossRef]
20. Chen, Y.; Du, W.; Dou, B.; Chen, J.; Hu, L.; Zeb, A.; Lin, X. Metal–organic frameworks and their derivatives as electrode materials for Li-ion batteries: A mini review. *CrystEngComm* **2022**, *24*, 2729–2743. [CrossRef]
21. Ye, Z.; Jiang, Y.; Li, L.; Wu, F.; Chen, R. Rational Design of MOF-Based Materials for Next-Generation Rechargeable Batteries. *Nano Micro Lett.* **2021**, *13*, 203. [CrossRef] [PubMed]
22. Lu, X.F.; Fang, Y.; Luan, D.; Lou, X.W.D. Metal−organic frameworks derived functional materials for electrochemical energy storage and conversion: A mini review. *Nano Lett.* **2021**, *21*, 1555–1565. [CrossRef] [PubMed]
23. Gordeeva, L.G.; Tu, Y.D.; Pan, Q.; Palash, M.L.; Saha, B.B.; Aristov, Y.I.; Wang, R.Z. Metal-organic frameworks for energy conversion and water harvesting: A bridge between thermal engineering and material science. *Nano Energy* **2021**, *84*, 105946. [CrossRef]
24. Chuhadiya, S.; Himanshu; Suthar, D.; Patel, S.L.; Dhaka, M.S. Metal organic frameworks as hybrid porous materials for energy storage and conversion devices: A review. *Coord. Chem. Rev.* **2021**, *446*, 214115. [CrossRef]
25. Verma, J.; Kumar, D. Metal-ion batteries for electric vehicles: Current state of the technology, issues and future perspectives. *Nanoscale Adv.* **2021**, *3*, 3384–3394. [CrossRef]
26. Qiu, T.; Liang, Z.; Guo, W.; Tabassum, H.; Gao, S.; Zou, R. Metal–Organic Framework-Based Materials for Energy Conversion and Storage. *ACS Energy Lett.* **2020**, *5*, 520–532. [CrossRef]
27. El Boutaybi, M.; Taleb, A.; Touzani, R.; Bahari, Z. Metal-organic frameworks based on pyrazole subunit for batteries applications: A systematic review. *Mater. Today Proc.* **2020**, *31*, S96–S102. [CrossRef]
28. Wang, H.; Zhang, N.; Li, S.; Ke, Q.; Li, Z.; Zhou, M. Metal-organic framework composites for energy conversion and storage. *J. Semicond.* **2020**, *41*, 091707. [CrossRef]
29. Indra, A.; Song, T.; Paik, U. Metal Organic Framework Derived Materials: Progress and Prospects for the Energy Conversion and Storage. *Adv. Mater.* **2018**, *30*, 1705146. [CrossRef]
30. Mehtab, T.; Yasin, G.; Arif, M.; Shakeel, M.; Korai, R.M.; Nadeem, M.; Muhammad, N.; Lu, X. Metal-organic frameworks for energy storage devices: Batteries and supercapacitors. *J. Energy Storage* **2019**, *21*, 632–646. [CrossRef]
31. Steele, B.C.H.; Heinzel, A. Materials for fuel-cell technologies. *Nature* **2001**, *414*, 345–352. [CrossRef] [PubMed]
32. Mekhilef, S.; Saidur, R.; Safari, A. Comparative study of different fuel cell technologies. *Renew. Sustain. Energy Rev.* **2012**, *16*, 981–989. [CrossRef]
33. Wang, Y.; Chen, K.S.; Mishler, J.; Cho, S.C.; Adroher, X.C. A review of polymer electrolyte membrane fuel cells: Technology, applications, and needs on fundamental research. *Appl. Energy* **2011**, *88*, 981–1007. [CrossRef]
34. Heinzel, A.; Barragán, V.M. A review of the state-of-the-art of the methanol crossover in direct methanol fuel cells. *J. Power Sources* **1999**, *84*, 70–74. [CrossRef]
35. Hjuler, H.A.; Aili, D.; Jensen, J.O. High temperature polymer electrolyte membrane fuel cells: Approaches, status, and perspectives. In *High Temperature Polymer Electrolyte Membrane Fuel Cells*; Springer: Berlin/Heidelberg, Germany, 2016; pp. 1–545.
36. Dicks, A.L. Molten carbonate fuel cells. *Curr. Opin. Solid State Mater. Sci.* **2004**, *8*, 379–383. [CrossRef]
37. Stonehart, P. Development of alloy electrocatalysts for phosphoric acid fuel cells (PAFC). *J. Appl. Electrochem.* **1992**, *22*, 995–1001. [CrossRef]
38. McLean, G.F.; Niet, T.; Prince-Richard, S.; Djilali, N. An assessment of alkaline fuel cell technology. *Int. J. Hydrogen Energy* **2002**, *27*, 507–526. [CrossRef]
39. Singhal, S.C. Advances in solid oxide fuel cell technology. *Solid State Ion.* **2000**, *135*, 305–313. [CrossRef]
40. Walkowiak-Kulikowska, J.; Wolska, J.; Koroniak, H. Polymers application in proton exchange membranes for fuel cells (PEMFCs). *Phys. Sci. Rev.* **2017**, *2*. [CrossRef]
41. Sadakiyo, M.; Yamada, T.; Kitagawa, H. Rational designs for highly proton-conductive metal-organic frameworks. *J. Am. Chem. Soc.* **2009**, *131*, 9906–9907. [CrossRef]
42. Nagao, Y.; Kubo, T.; Nakasuji, K.; Ikeda, R.; Kojima, T.; Kitagawa, H. Preparation and proton transport property of N,N′-diethyldithiooxamidatocopper coordination polymer. *Synth. Met.* **2005**, *154*, 89–92. [CrossRef]
43. Zhu, J.; Fang, Z.; Yang, X.; Chen, M.; Chen, Z.; Qiu, F.; Wang, M.; Liu, P.; Xu, Q.; Zhuang, X.; et al. Core–Shell Structured Fe–N–C Catalysts with Enriched Iron Sites in Surface Layers for Proton-Exchange Membrane Fuel Cells. *ACS Catal.* **2022**, *12*, 6409–6417. [CrossRef]
44. Zhu, L.; Li, Y.; Zhao, J.; Liu, J.; Wang, L.; Lei, J.; Xue, R. Enhanced proton conductivity of Nafion membrane induced by incorporation of MOF-anchored 3D microspheres: A superior and promising membrane for fuel cell applications. *Chem. Commun.* **2022**, *58*, 2906–2909. [CrossRef]

45. Taylor, J.M.; Dekura, S.; Ikeda, R.; Kitagawa, H. Defect control to enhance proton conductivity in a metal-organic framework. *Chem. Mater.* **2015**, *27*, 2286–2289. [CrossRef]
46. Asl, M.H.; Moosavi, F.; Akbari, S. Mixed membrane matrices (MMMs) based on Nafion® pristine/defected-UiO-66(Zr) MOFs: Assessment of the effects of dopants on cluster morphology. *Mol. Syst. Des. Eng.* **2022**, *7*, 969–985.
47. Si, G.R.; Yang, F.; He, T.; Kong, X.J.; Wu, W.; Li, T.C.; Wang, K.; Li, J.R. Enhancing proton conductivity in Zr-MOFs through tuning metal cluster connectivity. *J. Mater. Chem. A* **2022**, *10*, 1236–1240. [CrossRef]
48. Zhang, L.; Li, L.; Gao, Z.; Guo, L.; Li, M.; Su, J. Porous Hierarchical Iron/Nitrogen co-doped Carbon Etched by g-C3N4 Pyrolysis as Efficient Non-noble Metal Catalysts for PEM Fuel Cells. *ChemElectroChem* **2022**, *9*, e202101681. [CrossRef]
49. Xie, X.; Shang, L.; Xiong, X.; Shi, R.; Zhang, T. Fe Single-Atom Catalysts on MOF-5 Derived Carbon for Efficient Oxygen Reduction Reaction in Proton Exchange Membrane Fuel Cells. *Adv. Energy Mater.* **2022**, *12*, 2102688. [CrossRef]
50. Ponnada, S.; Kiai, M.S.; Gorle, D.B.; Nowduri, A.; Sharma, R.K. Insight into the Role and Strategies of Metal-Organic Frameworks in Direct Methanol Fuel Cells: A Review. *Energy Fuels* **2021**, *35*, 15265–15284. [CrossRef]
51. Raj, V. Direct methanol fuel cells in portable applications: Materials, designs, operating parameters, and practical steps toward commercialization. *Direct Methanol Fuel Cell Technol.* **2020**, 495–525. [CrossRef]
52. Duan, Y.; Ru, C.; Li, J.; Sun, Y.N.; Pu, X.; Liu, B.; Pang, B.; Zhao, C. Enhancing proton conductivity and methanol resistance of SPAEK membrane by incorporating MOF with flexible alkyl sulfonic acid for DMFC. *J. Memb. Sci.* **2022**, *641*, 119906. [CrossRef]
53. Noor, T.; Mohtashim, M.; Iqbal, N.; Naqvi, S.R.; Zaman, N.; Rasheed, L.; Yousuf, M. Graphene based FeO/NiO MOF composites for methanol oxidation reaction. *J. Electroanal. Chem.* **2021**, *890*, 115249. [CrossRef]
54. Liang, X.; Zhou, X.; Ge, C.; Lin, H.; Satapathi, S.; Zhu, Q.; Hu, H. Advance and prospect of metal-organic frameworks for perovskite photovoltaic devices. *Org. Electron.* **2022**, *106*, 106546. [CrossRef]
55. Lee, J.; Tsvetkov, N.; Shin, S.R.; Kang, J.K. Fast Charge Transfer and High Stability via Hybridization of Hygroscopic Cu-BTC Metal-Organic Framework Nanocrystals with a Light-Absorbing Layer for Perovskite Solar Cells. *ACS Appl. Mater. Interfaces* **2022**, *14*, 35495–35503. [CrossRef]
56. Zhang, J.; Li, J.; Yang, Y.; Yang, C.; Dong, Y.; Lin, K.; Xia, D.; Fan, R. Functionalized Rare-Earth Metal Cluster-Based Materials as Additives for Enhancing the Efficiency of Perovskite Solar Cells. *ACS Appl. Energy Mater.* **2022**, *2022*, 13318–13326. [CrossRef]
57. Rong, B.; Wei, Y.; Chen, X.; Ding, Y.; Chen, Y.; Liu, H.; Huang, Y.; Fan, L.; Wu, J. Electron transport improvement of perovskite solar cells via intercalation of Na doped TiO2 from metal-organic framework MIL-125(Ti). *Appl. Surf. Sci.* **2022**, *574*, 151735. [CrossRef]
58. Chen, L.; Chen, Q.; Wang, C.; Li, Y. Interfacial dipole in organic and perovskite solar cells. *J. Am. Chem. Soc.* **2020**, *142*, 18281–18292. [CrossRef]
59. Dong, Y.; Zhang, J.; Yang, Y.; Wang, J.; Hu, B.; Wang, W.; Cao, W.; Gai, S.; Xia, D.; Lin, K.; et al. Multifunctional nanostructured host-guest POM@MOF with lead sequestration capability induced stable and efficient perovskite solar cells. *Nano Energy* **2022**, *97*, 107184. [CrossRef]
60. Uğur, A.; Gencer Imer, A.; Gülcan, M. Enhancement in the photovoltaic efficiency of dye-sensitized solar cell by doping TiO_2 with MIL-101 MOF structure. *Mater. Sci. Semicond. Process.* **2022**, *150*, 106951. [CrossRef]
61. Selvaraj, B.; Shanmugam, G.; Kamaraj, S.; Thirugnanasambandam, E.; Gunasekeran, A.; Sambandam, A. Effect of an aqueous copper gel electrolyte with cobalt metal organic framework based additive on performance of aqueous-dye-sensitized solar cells. *Sol. Energy* **2022**, *236*, 586–598. [CrossRef]
62. Thong, C.H.; Priyanga, N.; Ng, F.L.; Pappathi, M.; Periasamy, V.; Phang, S.M. Metal organic frameworks (MOFs) as potential anode materials for improving power generation from algal biophotovoltaic (BPV) platforms. *Catal. Today* **2022**, *397–399*, 419–427. [CrossRef]
63. Nevruzoglu, V.; Demir, S.; Karaca, G.; Tomakin, M.; Bilgin, N.; Yilmaz, F. Improving the stability of solar cells using metal–organic frameworks. *J. Mater. Chem. A* **2016**, *4*, 7930–7935. [CrossRef]
64. Ifraemov, R.; Mukhopadhyay, S.; Rozenberg, I.; Hod, I. Metal-Organic-Framework-Based Photo-electrochemical Cells for Solar Fuel Generation. *J. Phys. Chem. C* **2022**, *126*, 5079–5091. [CrossRef]
65. Brodd, R.J.; Bullock, K.R.; Leising, R.A.; Middaugh, R.L.; Miller, J.R.; Takeuchi, E. Batteries, 1977 to 2002. *J. Electrochem. Soc.* **2004**, *151*, K1. [CrossRef]
66. Song, J.Y.; Wang, Y.Y.; Wan, C.C. Review of gel-type polymer electrolytes for lithium-ion batteries. *J. Power Sources* **1999**, *77*, 183–197. [CrossRef]
67. Waghorne, W.E. Viscosities of electrolyte solutions. *Philos. Trans. R. Soc. London. Ser. A Math. Phys. Eng. Sci.* **2001**, *359*, 1529–1543. [CrossRef]
68. Nitta, N.; Wu, F.; Lee, J.T.; Yushin, G. Li-ion battery materials: Present and future. *Mater. Today* **2015**, *18*, 252–264. [CrossRef]
69. Mechili, M.; Vaitsis, C.; Argirusis, N.; Pandis, P.K.; Sourkouni, G.; Zorpas, A.A.; Argirusis, C. Research Progress in Metal-Organic Framework Based Nanomaterials Applied in Battery Cathodes. *Energies* **2022**, *15*, 5460. [CrossRef]
70. Chen, W.; Liu, S.; Shen, J. A review of MOFs and its derivatives for lithium ion battery anodes. *IOP Conf. Ser. Earth Environ. Sci.* **2021**, *634*, 012042.

71. Cao, X.; Tan, C.; Sindoro, M.; Zhang, H. Hybrid micro-/nano-structures derived from metal–organic frameworks: Preparation and applications in energy storage and conversion. *Chem. Soc. Rev.* **2017**, *46*, 2660–2677. [CrossRef]
72. Xu, G.; Nie, P.; Dou, H.; Ding, B.; Li, L.; Zhang, X. Exploring metal organic frameworks for energy storage in batteries and supercapacitors. *Mater. Today* **2017**, *20*, 191–209. [CrossRef]
73. Kaneti, Y.V.; Tang, J.; Salunkhe, R.R.; Jiang, X.; Yu, A.; Wu, K.C.W.; Yamauchi, Y. Nanoarchitectured Design of Porous Materials and Nanocomposites from Metal-Organic Frameworks. *Adv. Mater.* **2017**, *29*, 1604898. [CrossRef] [PubMed]
74. Nzereogu, P.U.; Omah, A.D.; Ezema, F.I.; Iwuoha, E.I.; Nwanya, A.C. Anode materials for lithium-ion batteries: A review. *Appl. Surf. Sci. Adv.* **2022**, *9*, 100233. [CrossRef]
75. Bennett, T.D.; Tan, J.C.; Yue, Y.; Baxter, E.; Ducati, C.; Terrill, N.J.; Yeung, H.H.M.; Zhou, Z.; Chen, W.; Henke, S.; et al. Hybrid glasses from strong and fragile metal-organic framework liquids. *Nat. Commun.* **2015**, *6*, 8079. [CrossRef]
76. Sørensen, S.S.; Østergaard, M.B.; Stepniewska, M.; Johra, H.; Yue, Y.; Smedskjaer, M.M. Metal-Organic Framework Glasses Possess Higher Thermal Conductivity than Their Crystalline Counterparts. *ACS Appl. Mater. Interfaces* **2020**, *12*, 18893–18903. [CrossRef]
77. Gao, C.; Jiang, Z.; Qi, S.; Wang, P.; Rosgaard Jensen, L.; Johansen, M.; Kolle Christensen, C.; Zhang, Y.; Bomholdt Ravnsbaek, D.; Yue, Y.; et al. Metal-Organic Framework Glass Anode with an Exceptional Cycling-Induced Capacity Enhancement for Lithium-Ion Batteries. *Adv. Mater.* **2022**, *34*, 2110048. [CrossRef]
78. Cai, Y.; Wang, W.; Cao, X.; Wei, L.; Ye, C.; Meng, C.; Yuan, A.; Pang, H.; Yu, C.; Cai, Y.J.; et al. Synthesis of Tostadas-Shaped Metal-Organic Frameworks for Remitting Capacity Fading of Li-Ion Batteries. *Adv. Funct. Mater.* **2022**, *32*, 2109927. [CrossRef]
79. Li, C.; Zhang, C.; Xie, J.; Wang, K.; Li, J.; Zhang, Q. Ferrocene-based metal-organic framework as a promising cathode in lithium-ion battery. *Chem. Eng. J.* **2021**, *404*, 126463. [CrossRef]
80. Chen, Y.; Tang, M.; Wu, Y.; Su, X.; Li, X.; Xu, S.; Zhuo, S.; Ma, J.; Yuan, D.; Wang, C.; et al. A One-Dimensional π–d Conjugated Coordination Polymer for Sodium Storage with Catalytic Activity in Negishi Coupling. *Angew. Chemie* **2019**, *131*, 14873–14881. [CrossRef]
81. Xie, J.; Cheng, X.-F.; Cao, X.; He, J.-H.; Guo, W.; Li, D.-S.; Xu, Z.J.; Huang, Y.; Lu, J.-M.; Zhang, Q. Nanostructured Metal–Organic Conjugated Coordination Polymers with Ligand Tailoring for Superior Rechargeable Energy Storage. *Small* **2019**, *15*, 1903188. [CrossRef]
82. Li, C.; Zhang, C.; Wang, K.; Yu, F.; Xie, J.; Zhang, Q. Multi-thiol-supported dicarboxylate-based metal-organic framework with excellent performance for lithium-ion battery. *Chem. Eng. J.* **2022**, *431*, 133234. [CrossRef]
83. Yang, D.X.; Wang, P.F.; Liu, H.Y.; Zhang, Y.H.; Sun, P.P.; Shi, F.N. Facile synthesis of ternary transition metal-organic framework and its stable lithium storage properties. *J. Solid State Chem.* **2022**, *309*, 122947. [CrossRef]
84. Zheng, W.; Hu, T.; Fang, Y.; Li, L.; Yuan, W. High capacity of microspheric manganese and cobalt trimesic dual-metal organic framework for Li-ion battery. *J. Solid State Chem.* **2022**, *306*, 122719. [CrossRef]
85. Lv, X.N.; Zhang, Y.H.; Sun, P.P.; Wang, P.F.; Tang, J.J.; Yang, G.; Shi, Q.; Shi, F.N. One pot synthesis of lanthanide-iron-sodium trimetallic metal-organic frameworks as anode materials for lithium-ion batteries. *J. Solid State Chem.* **2022**, *306*, 122786. [CrossRef]
86. Zhu, Y.; Peng, L.; Fang, Z.; Yan, C.; Zhang, X.; Yu, G. Structural Engineering of 2D Nanomaterials for Energy Storage and Catalysis. *Adv. Mater.* **2018**, *30*, 1706347. [CrossRef]
87. Xiong, P.; Sun, B.; Sakai, N.; Ma, R.; Sasaki, T.; Wang, S.; Zhang, J.; Wang, G. 2D Superlattices for Efficient Energy Storage and Conversion. *Adv. Mater.* **2020**, *32*, 1902654. [CrossRef] [PubMed]
88. Pomerantseva, E.; Gogotsi, Y. Two-dimensional heterostructures for energy storage. *Nat. Energy* **2017**, *27*, 1–6. [CrossRef]
89. Zhang, H.; Hussain, I.; Brust, M.; Butler, M.F.; Rannard, S.P.; Cooper, A.I. Aligned two- and three-dimensional structures by directional freezing of polymers and nanoparticles. *Nat. Mater.* **2005**, *4*, 787–793. [CrossRef]
90. Wang, Y.; Li, J.; Li, X.; Jin, H.; Ali, W.; Song, Z.; Ding, S. Metal–organic-framework derived Co@CN modified horizontally aligned graphene oxide array as free-standing anode for lithium-ion batteries. *J. Mater. Chem. A* **2022**, *10*, 699–706. [CrossRef]
91. Zhou, Q.; Li, W.; Gao, M.; Xu, H.; Guo, Y.; Sun, L.; Zheng, D.; Lin, J. A truncated octahedron metal-organic framework derived TiO2@C@MoS2 composite with superior lithium-ion storage properties. *J. Power Sources* **2022**, *518*, 230746. [CrossRef]
92. Tang, Y.; Kang, H.; Zheng, J.; Li, H.; Wang, R.; Zhang, L.; Ma, Q.; Xiong, X.; Zhou, T.; Zhang, C. Metal-Organic Framework derived Bi2S3 hybrid nanofibers for enhanced lithium-ion storage. *J. Power Sources* **2022**, *520*, 230895. [CrossRef]
93. Moustafa, M.G.; Aboraia, A.M.; Butova, V.V.; Elmasry, F.; Guda, A.A. Facile synthesis of ZnNC derived from a ZIF-8 metal-organic framework by the microwave-assisted solvothermal technique as an anode material for lithium-ion batteries. *New J. Chem.* **2022**, *46*, 9138–9145. [CrossRef]
94. Wu, W.; Zhao, C.; Liu, H.; Liu, T.; Wang, L.; Zhu, J. Hierarchical architecture of two-dimensional Ti3C2 nanosheets@Metal-Organic framework derivatives as anode for hybrid li-ion capacitors. *J. Colloid Interface Sci.* **2022**, *623*, 216–225. [CrossRef] [PubMed]
95. Jiang, X.B.; Shao, M.Y.; Li, K.; Ding, L.; Zeng, M. Facile synthesis and lithium storage mechanism study of directly usable tin-based metal organic framework. *J. Electroanal. Chem.* **2022**, *912*, 116268. [CrossRef]
96. Liu, J.; Xie, D.; Xu, X.; Jiang, L.; Si, R.; Shi, W.; Cheng, P. Reversible formation of coordination bonds in Sn-based metal-organic frameworks for high-performance lithium storage. *Nat. Commun.* **2021**, *12*, 1–10. [CrossRef]
97. Yao, H.; Yan, L.; Shen, J.; Wang, T.; Chen, P.; Cong, X.; Zhang, S.; Jiang, H.; Zhao, X. Controllably regulating ion transport in lithium metal batteries via pore effect of metal–organic framework-based separators. *Appl. Surf. Sci.* **2022**, *589*, 152885. [CrossRef]

98. Tu, Z.; Choudhury, S.; Zachman, M.J.; Wei, S.; Zhang, K.; Kourkoutis, L.F.; Archer, L.A. Designing Artificial Solid-Electrolyte Interphases for Single-Ion and High-Efficiency Transport in Batteries. *Joule* **2017**, *1*, 394–406. [CrossRef]
99. Tu, Z.; Zachman, M.J.; Choudhury, S.; Wei, S.; Ma, L.; Yang, Y.; Kourkoutis, L.F.; Archer, L.A.; Tu, Z.; Ma, L.; et al. Nanoporous Hybrid Electrolytes for High-Energy Batteries Based on Reactive Metal Anodes. *Adv. Energy Mater.* **2017**, *7*, 1602367. [CrossRef]
100. Zhang, S.S. A review on the separators of liquid electrolyte Li-ion batteries. *J. Power Sources* **2007**, *164*, 351–364. [CrossRef]
101. Shen, L.; Wu, H.B.; Liu, F.; Zhang, C.; Ma, S.; Le, Z.; Lu, Y. Anchoring anions with metal–organic framework-functionalized separators for advanced lithium batteries. *Nanoscale Horiz.* **2019**, *4*, 705–711. [CrossRef]
102. Li, Z.; Wang, S.; Shi, J.; Liu, Y.; Zheng, S.; Zou, H.; Chen, Y.; Kuang, W.; Ding, K.; Chen, L.; et al. A 3D interconnected metal-organic framework-derived solid-state electrolyte for dendrite-free lithium metal battery. *Energy Storage Mater.* **2022**, *47*, 262–270. [CrossRef]
103. Wang, L.; Liu, J.; Yuan, S.; Wang, Y.; Xia, Y. To mitigate self-discharge of lithium–sulfur batteries by optimizing ionic liquid electrolytes. *Energy Environ. Sci.* **2016**, *9*, 224–231. [CrossRef]
104. Bhauriyal, P.; Heine, T. Catalysing the performance of Li–sulfur batteries with two-dimensional conductive metal organic frameworks. *J. Mater. Chem. A* **2022**, *10*, 12400–12408. [CrossRef]
105. Geng, P.; Du, M.; Guo, X.; Pang, H.; Tian, Z.; Braunstein, P.; Xu, Q. Bimetallic Metal-Organic Framework with High-Adsorption Capacity toward Lithium Polysulfides for Lithium–sulfur Batteries. *Energy Environ. Mater.* **2022**, *5*, 599–607. [CrossRef]
106. Hu, X.; Huang, Q.; Zhang, Y.; Zhong, H.; Lin, Z.; Lin, X.; Zeb, A.; Xu, C.; Xu, X. A metal–organic framework approach to engineer mesoporous ZnMnO 3/C towards enhanced lithium storage. *Sustain. Energy Fuels* **2022**, *6*, 1175–1185. [CrossRef]
107. Shi, X.; Lei, D.; Qiao, S.; Zhang, Q.; Wang, Q.; Deng, X.; Liu, J.; He, G.; Zhang, F. Metal-Organic Framework-Derived NiSe2Nanoparticles on Graphene for Polysulfide Conversion in Lithium-Sulfur Batteries. *ACS Appl. Nano Mater.* **2022**, *16*, 6.
108. Chen, X.; Li, L.; Shan, Y.; Zhou, D.; Cui, W.; Zhao, Y. Synergistic effect of cerium oxide with core-shell structure embedded in porous carbon for high-performance lithium-sulfur batteries. *Mater. Today Commun.* **2021**, *27*, 102381. [CrossRef]
109. Feng, W.; Chen, J.; Niu, Y.; Zhao, W.; Zhang, L. CeO2 composite metal organic framework is used to construct high-performance lithium-sulfur batteries. *J. Alloys Compd.* **2022**, *906*, 164341. [CrossRef]
110. Zeng, Q.; Li, X.; Gong, W.; Guo, S.; Ouyang, Y.; Li, D.; Xiao, Y.; Tan, C.; Xie, L.; Lu, H.; et al. Copolymerization of Sulfur Chains with Vinyl Functionalized Metal−Organic Framework for Accelerating Redox Kinetics in Lithium−Sulfur Batteries. *Adv. Energy Mater.* **2022**, *12*, 2104074. [CrossRef]
111. Capková, D.; Kazda, T.; Čech, O.; Király, N.; Zelenka, T.; Čudek, P.; Sharma, A.; Hornebecq, V.; Fedorková, A.S.; Almáši, M. Influence of metal-organic framework MOF-76(Gd) activation/carbonization on the cycle performance stability in Li-S battery. *J. Energy Storage* **2022**, *51*, 104419. [CrossRef]
112. Chen, D.; Mukherjee, S.; Zhang, C.; Li, Y.; Xiao, B.; Singh, C.V. Two-dimensional square metal organic framework as promising cathode material for lithium-sulfur battery with high theoretical energy density. *J. Colloid Interface Sci.* **2022**, *613*, 435–446. [CrossRef]
113. Li, Y.; Lu, Y.; Zhao, C.; Hu, Y.S.; Titirici, M.M.; Li, H.; Huang, X.; Chen, L. Recent advances of electrode materials for low-cost sodium-ion batteries towards practical application for grid energy storage. *Energy Storage Mater.* **2017**, *7*, 130–151. [CrossRef]
114. He, H.; Sun, D.; Tang, Y.; Wang, H.; Shao, M. Understanding and improving the initial Coulombic efficiency of high-capacity anode materials for practical sodium ion batteries. *Energy Storage Mater.* **2019**, *23*, 233–251. [CrossRef]
115. Kim, S.W.; Seo, D.H.; Ma, X.; Ceder, G.; Kang, K. Electrode Materials for Rechargeable Sodium-Ion Batteries: Potential Alternatives to Current Lithium-Ion Batteries. *Adv. Energy Mater.* **2012**, *2*, 710–721. [CrossRef]
116. Zhang, M.; Li, Y.; Wu, F.; Bai, Y.; Wu, C. Boost sodium-ion batteries to commercialization: Strategies to enhance initial Coulombic efficiency of hard carbon anode. *Nano Energy* **2021**, *82*, 105738. [CrossRef]
117. Chen, W.; Zhang, X.; Mi, L.; Liu, C.; Zhang, J.; Cui, S.; Feng, X.; Cao, Y.; Shen Chen, C.W.; Zhang, X.; et al. High-Performance Flexible Freestanding Anode with Hierarchical 3D Carbon-Networks/Fe7S8/Graphene for Applicable Sodium-Ion Batteries. *Adv. Mater.* **2019**, *31*, 1806664. [CrossRef]
118. Ma, Y.; Ma, Y.; Giuli, G.; Diemant, T.; Behm, R.J.; Geiger, D.; Kaiser, U.; Ulissi, U.; Passerini, S.; Bresser, D. Conversion/alloying lithium-ion anodes—Enhancing the energy density by transition metal doping. *Sustain. Energy Fuels* **2018**, *2*, 2601–2608. [CrossRef]
119. Sanati, S.; Morsali, A.; Garcia, H. First-row transition metal-based materials derived from bimetallic metal–organic frameworks as highly efficient electrocatalysts for electrochemical water splitting. *Energy Environ. Sci.* **2022**, *15*, 3119–3151. [CrossRef]
120. Li, X.; Yang, X.; Xue, H.; Pang, H.; Xu, Q. Metal–organic frameworks as a platform for clean energy applications. *EnergyChem* **2020**, *2*, 100027. [CrossRef]
121. Yu, M.; Dong, R.; Feng, X. Two-Dimensional Carbon-Rich Conjugated Frameworks for Electrochemical Energy Applications. *J. Am. Chem. Soc.* **2020**, *142*, 12903–12915. [CrossRef]
122. Fan, K.; Zhang, C.; Chen, Y.; Wu, Y.; Wang, C. The chemical states of conjugated coordination polymers. *Chem* **2021**, *7*, 1224–1243. [CrossRef]
123. Wang, B.; Li, J.; Ye, M.; Zhang, Y.; Tang, Y.; Hu, X.; He, J.; Chao Li, C.; Wang, B.; Li, J.; et al. Dual-Redox Sites Guarantee High-Capacity Sodium Storage in Two-Dimension Conjugated Metal–Organic Frameworks. *Adv. Funct. Mater.* **2022**, *32*, 2112072. [CrossRef]

124. Zhang, Y.; Chen, K.; Guo, H.; Huang, Y.; Li, W.; Wang, C.; Wang, Y. Phase transformation induced benzene rings activation in a metal–organic framework to boost sodium storage performance. *Chem. Eng. J.* **2022**, *433*, 133508. [CrossRef]
125. Zhang, Y.J.; Gao, Y.J.; Wang, X.; Ye, Q.; Zhang, Y.; Wu, Y.; Chen, S.H.; Ruan, B.; Shi, D.; Jiang, T.; et al. $MoTe_2$ on metal-organic framework derived MoO2/N-doped carbon rods for enhanced sodium-ion storage properties. *Energy* **2022**, *243*, 123043. [CrossRef]
126. Chen, L.; Wang, X.; Ding, Y.; Li, Y.; Ren, S.B.; Shen, M.; Chen, Y.X.; Li, W.; Han, D.M. Metal–organic framework-derived nitrogen-doped carbon-confined $CoSe_2$ anchored on multiwalled carbon nanotube networks as an anode for high-rate sodium-ion batteries. *Dalt. Trans.* **2022**, *51*, 5184–5194. [CrossRef]
127. Feng, J.; Luo, S.H.; Lin, Y.; Zhan, Y.; Yan, S.; Hou, P.; Wang, Q.; Zhang, Y. hui. Metal-organic framework derived CoSe2/N-doped carbon core-shell nanoparticles encapsulated in porous N-doped carbon nanotubes as high-performance anodes for sodium-ion batteries. *J. Power Sources* **2022**, *535*, 231444. [CrossRef]
128. Zhu, H.; Li, Z.; Xu, F.; Qin, Z.; Sun, R.; Wang, C.; Lu, S.; Zhang, Y.; Fan, H. Ni3Se4@CoSe2 hetero-nanocrystals encapsulated into CNT-porous carbon interpenetrating frameworks for high-performance sodium ion battery. *J. Colloid Interface Sci.* **2022**, *611*, 718–725. [CrossRef]
129. Qian, Z.; Wang, X.; Liu, T.; Zhang, L.; Yu, J. Nickel-cobalt selenide@N-doped carbon towards high-performance anode materials for sodium-ion batteries. *J. Energy Storage* **2022**, *51*, 104522. [CrossRef]
130. Huang, Y.; Wang, M.; Huang, M.; Xiong, Y.; Yang, X.; Miao, Z.; Yang, Z.; Yu, J. Co0.85Se@carbon nanotubes surface-seeding grown on carbon microplates as superior anode material for sodium ion batteries. *Electrochim. Acta* **2022**, *414*, 140167. [CrossRef]
131. Ma, Y.; Chen, X.; Cao, P.; Wang, Y.; Li, F.; Li, L.; Zhang, W. Employing ZIF-67 architectures into 1D binder-free Co3O4-based carbon fiber composites for advanced sodium-ion storage application. *J. Alloys Compd.* **2022**, *890*, 161907. [CrossRef]
132. Liang, H.; Li, X.; Liu, X.; Sun, R.; Qin, Z.; Zhang, Y.; Fan, H. Epitaxial growth induced multilayer yolk-shell structured CoSe2 with promoting transport kinetics of sodium ion half/full batteries. *J. Power Sources* **2022**, *517*, 230729. [CrossRef]
133. Wang, L.; Liu, B.; Zhu, Y.; Yang, M.; Du, C.; Han, Z.; Yao, X.; Ma, X.; Cao, C. General metal–organic framework-derived strategy to synthesize yolk-shell carbon-encapsulated nickelic spheres for sodium-ion batteries. *J. Colloid Interface Sci.* **2022**, *613*, 23–34. [CrossRef]
134. Li, H.; Zhang, H.; Zarrabeitia, M.; Liang, H.-P.; Geiger, D.; Kaiser, U.; Varzi, A.; Passerini, S.; Li, H.; Zhang, H.; et al. Metal–Organic Framework Derived Copper Chalcogenides-Carbon Composites as High-Rate and Stable Storage Materials for Na Ions. *Adv. Sustain. Syst.* **2022**, *6*, 2200109. [CrossRef]
135. Chen, J.-J.; Ye, J.-C.; Zhang, X.-G.; Symes, M.D.; Fan, S.-C.; Long, D.-L.; Zheng, M.-S.; Wu, D.-Y.; Cronin, L.; Dong, Q.-F.; et al. Design and Performance of Rechargeable Sodium Ion Batteries, and Symmetrical Li-Ion Batteries with Supercapacitor-Like Power Density Based upon Polyoxovanadates. *Adv. Energy Mater* **2018**, *8*, 1701021. [CrossRef]
136. Cao, D.; Sha, Q.; Wang, J.; Li, J.; Ren, J.; Shen, T.; Bai, S.; He, L.; Song, Y.F. Advanced Anode Materials for Sodium-Ion Batteries: Confining Polyoxometalates in Flexible Metal-Organic Frameworks by the 'breathing Effect'. *ACS Appl. Mater. Interfaces* **2022**, *14*, 22186–22196. [CrossRef]
137. Wang, J.; Yue, X.; Liu, Z.; Xie, Z.; Zhao, Q.; Abudula, A.; Guan, G. Trimetallic sulfides derived from tri-metal-organic frameworks as anode materials for advanced sodium ion batteries. *J. Colloid Interface Sci.* **2022**, *625*, 248–256. [CrossRef]
138. Li, C.; Li, A.; Li, M.; Xiong, P.; Liu, Y.; Cheng, M.; Geng, D.; Xu, Y. Ultrafast Synthesis of Layered Transition-Metal Oxide Cathodes from Metal–Organic Frameworks for High-Capacity Sodium-Ion Batteries. *ACS Appl. Mater. Interfaces* **2022**, *14*, 24462–24468. [CrossRef]
139. Yang, C.; Shang, S.; Gu, Q.; Shang, J.; Li, X. Metal-organic framework-derived carbon nanotubes with multi-active Fe-N/Fe sites as a bifunctional electrocatalyst for zinc-air battery. *J. Energy Chem.* **2022**, *66*, 306–313. [CrossRef]
140. Shin, S.; Yoon, Y.; Shin, M.W. Co/Zn-based bimetallic MOF-derived hierarchical porous Co/C composite as cathode material for high-performance lithium-air batteries. *Int. J. Energy Res.* **2022**, *46*, 9900–9910. [CrossRef]
141. Dong, X.; Sun, J.; Mu, Y.; Yu, Y.; Hu, T.; Miao, C.; Huang, C.; Meng, C.; Zhang, Y. RGO/Manganese Silicate/MOF-derived carbon Double-Sandwich-Like structure as the cathode material for aqueous rechargeable Zn-ion batteries. *J. Colloid Interface Sci.* **2022**, *610*, 805–817. [CrossRef]
142. Zhang, J.; Chen, Y.; Liu, Y.; Liu, X.; Gao, S. Self-catalyzed growth of Zn/Co-N-C carbon nanotubes derived from metal-organic frameworks as efficient oxygen reduction catalysts for Zn-air battery. *Sci. China Mater.* **2021**, *65*, 653–662. [CrossRef]
143. Suntivich, J.; Gasteiger, H.A.; Yabuuchi, N.; Nakanishi, H.; Goodenough, J.B.; Shao-Horn, Y. Design principles for oxygen-reduction activity on perovskite oxide catalysts for fuel cells and metal–air batteries. *Nat. Chem.* **2011**, *3*, 546–550. [CrossRef] [PubMed]
144. He, B.; Deng, Y.; Wang, H.; Wang, R.; Jin, J.; Gong, Y.; Zhao, L. Metal organic framework derived perovskite/spinel heterojunction as efficient bifunctional oxygen electrocatalyst for rechargeable and flexible Zn-air batteries. *J. Colloid Interface Sci.* **2022**, *625*, 502–511. [CrossRef] [PubMed]
145. Díaz, R.; Orcajo, M.G.; Botas, J.A.; Calleja, G.; Palma, J. Co8-MOF-5 as electrode for supercapacitors. *Mater. Lett.* **2012**, *68*, 126–128. [CrossRef]

146. Lee, D.Y.; Yoon, S.J.; Shrestha, N.K.; Lee, S.H.; Ahn, H.; Han, S.H. Unusual energy storage and charge retention in Co-based metal–organic-frameworks. *Microporous Mesoporous Mater.* **2012**, *153*, 163–165. [CrossRef]
147. Arafat, Y.; Azhar, M.R.; Zhong, Y.; Xu, X.; Tadé, M.O.; Shao, Z. A Porous Nano-Micro-Composite as a High-Performance Bi-Functional Air Electrode with Remarkable Stability for Rechargeable Zinc–Air Batteries. *Nano-Micro Lett.* **2020**, *12*, 1–16. [CrossRef]
148. Zheng, Y.; Zheng, S.; Xu, Y.; Xue, H.; Liu, C.; Pang, H. Ultrathin two-dimensional cobalt-organic frameworks nanosheets for electrochemical energy storage. *Chem. Eng. J.* **2019**, *373*, 1319–1328. [CrossRef]
149. Hong, Y.; Wang, Y.; Guo, Y.; Wang, K.; Wu, H.; Zhang, C.; Zhang, Q. Recent advances in pillar-layered metal-organic frameworks with interpenetrated and non-interpenetrated topologies as supercapacitor electrodes. *Zeitschrift für Anorg. und Allg. Chemie* **2022**, *648*, e202200115. [CrossRef]
150. Pakulski, D.; Montes-García, V.; Gorczyński, A.; Czepa, W.; Chudziak, T.; Samorì, P.; Ciesielski, A. Thiol-decorated covalent organic frameworks as multifunctional materials for high-performance supercapacitors and heterogeneous catalysis. *J. Mater. Chem. A* **2022**, *10*, 16685–16696. [CrossRef]
151. Wang, S.; Guo, Y.Z.; Wang, F.X.; Zhou, S.H.; Zeng, T.Y.; Dong, Y. Research progress on metal and covalent organic framework-based materials for high-performance supercapacitors. *New Carbon Mater.* **2022**, *37*, 109–135. [CrossRef]
152. Umezawa, S.; Douura, T.; Yoshikawa, K.; Tanaka, D.; Stolojan, V.; Silva, S.R.P.; Yoneda, M.; Gotoh, K.; Hayashi, Y. Zinc-Based Metal–Organic Frameworks for High-Performance Supercapacitor Electrodes: Mechanism Underlying Pore Generation. *Energy Environ. Mater.* **2022**, 1–13. [CrossRef]
153. Yao, S.; Jiao, Y.; Sun, S.; Wang, L.; Li, P.; Chen, G. Vertically Co-oriented Mn-Metal-Organic Framework Grown on 2D Cation-Intercalated Manganese Oxide via a Self-sacrificing Template Process for a High-Performance Asymmetric Supercapacitor. *ACS Sustain. Chem. Eng.* **2020**, *8*, 3191–3199. [CrossRef]
154. Shi, C.; Kang, N.; Wang, C.; Yu, K.; Lv, J.; Wang, C.; Zhou, B. An inorganic–organic hybrid nanomaterial with a core–shell structure constructed by using Mn–BTC and $Ag_5[BW_{12}O_{40}]$ for supercapacitors and photocatalytic dye degradation. *Nanoscale Adv.* **2022**, *4*, 4358–4365. [CrossRef]
155. Xu, L.; Zhao, X.; Yu, K.; Wang, C.; Lv, J.; Wang, C.; Zhou, B. Simple preparation of Ag-BTC-modified $Co_3Mo_7O_{24}$ mesoporous material for capacitance and H_2O_2 -sensing performances. *CrystEngComm* **2022**, *24*, 5614–5621. [CrossRef]
156. Zheng, S.; Sun, Y.; Xue, H.; Braunstein, P.; Huang, W.; Pang, H. Dual-ligand and hard-soft-acid-base strategies to optimize metal-organic framework nanocrystals for stable electrochemical cycling performance. *Natl. Sci. Rev.* **2022**, *9*, nwab197. [CrossRef]
157. Sahoo, R.; Ghosh, S.; Chand, S.; Chand Pal, S.; Kuila, T.; Das, M.C. Highly scalable and pH sTable 2D Ni-MOF-based composites for high performance supercapacitor. *Compos. Part B Eng.* **2022**, *245*, 110174. [CrossRef]
158. Lu, J.; Duan, H.; Zhang, Y.; Zhang, G.; Chen, Z.; Song, Y.; Zhu, R.; Pang, H. Directional Growth of Conductive Metal-Organic Framework Nanoarrays along [001] on Metal Hydroxides for Aqueous Asymmetric Supercapacitors. *ACS Appl. Mater. Interfaces* **2022**, *14*, 25878–25885. [CrossRef]
159. Kumari, V.; Pal Singh, P.; Kaushal, S. Synthesis and applications of metal-organic frameworks and graphene-based composites: A review. *Polyhedron* **2022**, *214*, 115645. [CrossRef]
160. Rahmanifar, M.S.; Hesari, H.; Noori, A.; Masoomi, M.Y.; Morsali, A.; Mousavi, M.F. A dual Ni/Co-MOF-reduced graphene oxide nanocomposite as a high performance supercapacitor electrode material. *Electrochim. Acta* **2018**, *275*, 76–86. [CrossRef]
161. Gupta, A.K.; Saraf, M.; Bharadwaj, P.K.; Mobin, S.M. Dual Functionalized CuMOF-Based Composite for High-Performance Supercapacitors. *Inorg. Chem.* **2019**, *58*, 9844–9854. [CrossRef]
162. Yan, Y.; Luo, Y.; Ma, J.; Li, B.; Xue, H.; Pang, H.; Yan, Y.; Luo, Y.; Ma, J.; Li, B.; et al. Facile Synthesis of Vanadium Metal-Organic Frameworks for High-Performance Supercapacitors. *Small* **2018**, *14*, 1801815. [CrossRef]
163. Zaman, N.; Noor, T.; Iqbal, N. Recent advances in the metal–organic framework-based electrocatalysts for the hydrogen evolution reaction in water splitting: A review. *RSC Adv.* **2021**, *11*, 21904–21925. [CrossRef]
164. Khan, S.; Noor, T.; Iqbal, N.; Pervaiz, E. Recent Advancement in Metal-Organic Framework for Water Electrolysis: A Review. *ChemNanoMat* **2022**, *8*, e202200115. [CrossRef]
165. Budnikova, Y.H. Recent advances in metal–organic frameworks for electrocatalytic hydrogen evolution and overall water splitting reactions. *Dalt. Trans.* **2020**, *49*, 12483–12502. [CrossRef]
166. Tan, J.B.; Li, G.R. Recent progress on metal-organic frameworks and their derived materials for electrocatalytic water splitting. *J. Mater. Chem. A* **2022**, *8*, 14326–14355. [CrossRef]
167. Li, X.; Wang, Z.; Wang, L. Metal–Organic Framework-Based Materials for Solar Water Splitting. *Small Sci.* **2021**, *1*, 2000074. [CrossRef]
168. Jaryal, R.; Kumar, R.; Khullar, S. Mixed metal-metal organic frameworks (MM-MOFs) and their use as efficient photocatalysts for hydrogen evolution from water splitting reactions. *Coord. Chem. Rev.* **2022**, *464*, 214542. [CrossRef]
169. Cao, L.M.; Zhang, J.; Ding, L.W.; Du, Z.Y.; He, C.T. Metal-organic frameworks derived transition metal phosphides for electrocatalytic water splitting. *J. Energy Chem.* **2022**, *68*, 494–520. [CrossRef]
170. Zhang, P.F.; Wu, D.; Yang, G.P.; Wang, Y.Y. Metal-Organic Frameworks as Heterogeneous Electrocatalysts for Water Splitting and CO2Fixation. *Cryst. Growth Des.* **2021**, *21*, 3123–3142. [CrossRef]

171. Guan, J.; Pal, T.; Kamiya, K.; Fukui, N.; Maeda, H.; Sato, T.; Suzuki, H.; Tomita, O.; Nishihara, H.; Abe, R.; et al. Two-Dimensional Metal-Organic Framework Acts as a Hydrogen Evolution Cocatalyst for Overall Photocatalytic Water Splitting. *ACS Catal.* **2022**, *12*, 3881–3889. [CrossRef]
172. Zhang, Y.; Wen, C.; Wu, X.; Liu, P.F.; Yang, H.G. Reverse Replacement in NH2-MIL-125 with 1,4-Dicarboxybenzene for Enhanced Photocatalytic Hydrogen Generation. *Chem.—A Eur. J.* **2022**, *28*, e202200938. [CrossRef]
173. Wang, F.; Zhao, D.; Li, B.; Li, W.; Zhang, H.; Pang, J.; Fan, L. Compositional Engineering of Co(II)MOF/Carbon-Based Overall Water Splitting Electrocatalysts: From Synergistic Effects to Structure-Activity Relationships. *Cryst. Growth Des.* **2022**, *22*, 2775–2792. [CrossRef]
174. Gao, J.; Yu, X.; Li, Y.; Ma, Y. Structural Fine-Tuning and In-situ Generation of P, O Vacancies in Hollow Co-Ferrocene-MOFs Derived Phosphides for Efficient Water Oxidation. *ChemCatChem* **2022**, *14*, e202200558. [CrossRef]
175. Dai, S.; Liu, Y.; Mei, Y.; Hu, J.; Wang, K.; Li, Y.; Jin, N.; Wang, X.; Luo, H.; Li, W. Iron-doped novel Co-based metal–organic frameworks for preparation of bifunctional catalysts with an amorphous structure for OER/HER in alkaline solution. *Dalt. Trans.* **2022**, *51*, 15446–15457. [CrossRef]
176. Huang, P.; Miao, X.; Wu, J.; Zhang, P.; Zhang, H.; Bai, S.; Liu, W. Facile synthesis of an ultrathin ZIF-67 layer on the surface of Sn/Ti co-doped hematite for efficient photoelectrochemical water oxidation. *Dalt. Trans.* **2022**, *51*, 8848–8854. [CrossRef]
177. Liu, L.; Du, S.; Guo, X.; Xiao, Y.; Yin, Z.; Yang, N.; Bao, Y.; Zhu, X.; Jin, S.; Feng, Z.; et al. Water-Stable Nickel Metal-Organic Framework Nanobelts for Cocatalyst-Free Photocatalytic Water Splitting to Produce Hydrogen. *J. Am. Chem. Soc.* **2022**, *144*, 2747–2754. [CrossRef]
178. Li, Y.; Wang, Q.; Hu, X.; Meng, Y.; She, H.; Wang, L.; Huang, J.; Zhu, G. Constructing NiFe-metal-organic frameworks from NiFe-layered double hydroxide as a highly efficient cocatalyst for BiVO4 photoanode PEC water splitting. *Chem. Eng. J.* **2022**, *433*, 133592. [CrossRef]
179. Chhetri, K.; Muthurasu, A.; Dahal, B.; Kim, T.; Mukhiya, T.; Chae, S.H.; Ko, T.H.; Choi, Y.C.; Kim, H.Y. Engineering the abundant heterointerfaces of integrated bimetallic sulfide-coupled 2D MOF-derived mesoporous CoS_2 nanoarray hybrids for electrocatalytic water splitting. *Mater. Today Nano* **2022**, *17*, 100146. [CrossRef]
180. Ali, M.; Pervaiz, E. Effect of synthesis route on electrocatalytic water-splitting activity of MoS_2/UiO-66 hybrid. *Mol. Catal.* **2022**, *519*, 112136. [CrossRef]
181. Li, T.M.; Hu, B.Q.; Han, J.H.; Lu, W.; Yu, F.; Li, B. Highly Effective OER Electrocatalysts Generated from a Two-Dimensional Metal-Organic Framework Including a Sulfur-Containing Linker without Doping. *Inorg. Chem.* **2022**, *61*, 7051–7059. [CrossRef]
182. Yin, Z.; Liang, J.; Zhang, Z.Y.; Luo, H.; Zhou, J. Construction of superhydrophilic metal-organic frameworks with hierarchical microstructure for efficient overall water splitting. *J. Colloid Interface Sci.* **2022**, *623*, 405–416. [CrossRef]
183. Yu, H.; Wang, L.; Li, H.; Luo, Z.; Isimjan, T.T.; Yang, X. Improving the Electrocatalytic Activity of a Nickel-Organic Framework toward the Oxygen Evolution Reaction through Vanadium Doping. *Chem. A Eur. J.* **2022**, *28*, e202201784. [CrossRef]
184. Ali, M.; Pervaiz, E.; Rabi, O. Enhancing the Overall Electrocatalytic Water-Splitting Efficiency of Mo_2C Nanoparticles by Forming Hybrids with UiO-66 MOF. *ACS Omega* **2021**, *6*, 34219–34228. [CrossRef]
185. Shi, L.; Wu, C.; Wang, Y.; Dou, Y.; Yuan, D.; Li, H.; Huang, H.; Zhang, Y.; Gates, I.D.; Sun, X.; et al. Rational Design of Coordination Bond Connected Metal Organic Frameworks/MXene Hybrids for Efficient Solar Water Splitting. *Adv. Funct. Mater.* **2022**, *32*, 2202571. [CrossRef]
186. Lu, C.; Xiong, D.; Chen, C.; Wang, J.; Kong, Y.; Liu, T.; Ying, S.; Yi, F.Y. Indium-Based Metal-Organic Framework for Efficient Photocatalytic Hydrogen Evolution. *Inorg. Chem.* **2022**, *61*, 2587–2594. [CrossRef]
187. Ibomcha Singh, T.; Rajeshkhanna, G.; Narayan Pan, U.; Kshetri, T.; Lin, H.; Hoon Kim, N.; Hee Lee, J.; Singh, T.I.; Pan, U.N.; Kshetri, T.; et al. Alkaline Water Splitting Enhancement by MOF-Derived Fe–Co–Oxide/Co@NC-mNS Heterostructure: Boosting OER and HER through Defect Engineering and In Situ Oxidation. *Small* **2021**, *17*, 2101312. [CrossRef]
188. Liu, S.; Xiao, W.; Jin, C.; Xia, S.; Wang, W.; Jiang, X.; Li, L.; Wang, S.; Chen, C. MOFs derived CdS/CdO heterojunction photoanode for high-efficient water splitting. *Appl. Surf. Sci.* **2022**, *605*, 154697. [CrossRef]
189. Xu, Y.; Xie, M.; Li, X.; Shao, F.; Li, S.; Li, S.; Xu, Y.; Chen, J.; Zeng, F.; Jiao, Y. Regulating the electronic structure of Fe-based metal organic frameworks by electrodeposition of Au nanoparticles for electrochemical overall water splitting. *J. Colloid Interface Sci.* **2022**, *626*, 426–434. [CrossRef]
190. Li, S.; Wang, L.; Su, H.; Hong, A.N.; Wang, Y.; Yang, H.; Ge, L.; Song, W.; Liu, J.; Ma, T.; et al. Electron Redistributed S-Doped Nickel Iron Phosphides Derived from One-Step Phosphatization of MOFs for Significantly Boosting Electrochemical Water Splitting. *Adv. Funct. Mater.* **2022**, *32*, 2200733. [CrossRef]
191. Kong, Y.; Xiong, D.; Lu, C.; Wang, J.; Liu, T.; Ying, S.; Ma, X.; Yi, F.Y. Vanadium-Based Trimetallic Metal-Organic-Framework Family as Extremely High-Performing and Ultrastable Electrocatalysts for Water Splitting. *ACS Appl. Mater. Interfaces* **2022**, *14*, 37804–37813. [CrossRef]
192. Van Phuc, T.; Jana, J.; Ravi, N.; Kang, S.G.; Chung, J.S.; Choi, W.M.; Hur, S.H. Highly active Ni/Co-metal organic framework bifunctional electrocatalyst for water splitting reaction. *Int. J. Hydrogen Energy* **2022**, *47*, 22787–22795. [CrossRef]
193. Bhattacharjee, S.; Bera, S.; Das, R.; Chakraborty, D.; Basu, A.; Banerjee, P.; Ghosh, S.; Bhaumik, A. A Ni(II) Metal-Organic Framework with Mixed Carboxylate and Bipyridine Ligands for Ultrafast and Selective Sensing of Explosives and Photoelectrochemical Hydrogen Evolution. *ACS Appl. Mater. Interfaces* **2022**, *14*, 54. [CrossRef] [PubMed]

194. Li, D.; Shi, X.; Sun, S.; Zheng, X.; Tian, D.; Jiang, D. Metal-Organic Framework-Derived Three-Dimensional Macropore Nitrogen-Doped Carbon Frameworks Decorated with Ultrafine Ru-Based Nanoparticles for Overall Water Splitting. *Inorg. Chem.* **2022**, *61*, 9685–9692. [CrossRef] [PubMed]
195. Liu, D.; Wang, C.; Zhou, Z.; Ye, C.; Yu, R.; Wang, C.; Du, Y. Ultra-low Ru doped MOF-derived hollow nanorods for efficient oxygen evolution reaction. *Inorg. Chem. Front.* **2022**, *9*, 6158–6166. [CrossRef]
196. Wang, R.; Sun, P.; Yuan, Q.; Nie, R.; Wang, X. MOF-derived cobalt-embedded nitrogen-doped mesoporous carbon leaf for efficient hydrogen evolution reaction in both acidic and alkaline media. *Int. J. Hydrogen Energy* **2019**, *44*, 11838–11847. [CrossRef]
197. Zhao, R.; Liang, Z.; Zou, R.; Xu, Q. Metal-Organic Frameworks for Batteries. *Joule* **2018**, *2*, 2235–2259. [CrossRef]
198. Jiang, Y.; Zhao, H.; Yue, L.; Liang, J.; Li, T.; Liu, Q.; Luo, Y.; Kong, X.; Lu, S.; Shi, X.; et al. Recent advances in lithium-based batteries using metal organic frameworks as electrode materials. *Electrochem. Comm.* **2021**, *122*, 106881. [CrossRef]
199. Cui, X.; Dong, H.; Chen, S.; Wu, M.; Wang, Y. Progress and Perspective of Metal- and Covalent-Organic Frameworks and their Derivatives for Lithium-Ion Batteries. *Batter. Supercaps.* **2021**, *4*, 72–97. [CrossRef]